Pore pressure evolution in deforming granular material: A general formulation and the infinitely stiff approximation

L. Goren,[1] E. Aharonov,[2] D. Sparks,[3] R. Toussaint[4,5]

L. Goren, Department of Environmental Sciences and Energy Research, Weizmann Institute of Science, Rehovot 76100, Israel. (liran.goren@weizmann.ac.il)

E. Aharonov, Institute of Earth Sciences, Hebrew University, Givat Ram, Jerusalem 91904, Israel. (einatah@cc.huji.ac.il)

D. W. Sparks, Department of Geology and Geophysics, Texas A&M University, College Station, TX 77843-3115, USA. (sparks@geo.tamu.edu)

R. Toussaint, IPGS, CNRS UMR7516, 5 rue René Descartes, 67084 Strasbourg Cedex, France. (renaud.toussaint@eost.u-strasbg.fr)

[1]Department of Environmental Sciences

Abstract. Deformation of fluid-filled granular media occurs in many geophysical systems ranging from shear on geological faults to landslides and soil liquefaction. Its great complexity is rooted in the mechanical coupling between two deforming phases: the solid granular network and the fluid-filled pore network. Often deformation of the granular network leads to pore fluid pressure (PP) changes. If the PP rises enough, the fluid-filled granular media may transition from a stress-supporting grain network to a flowing grain-fluid slurry, with an accompanying catastrophic loss of shear strength. Despite its great importance, the mechanisms and parameters controlling PP evolution by granular shear are not well understood. A formulation describ-

and Energy Research, Weizmann Institute of Science, Rehovot, Israel.

[2]Institute of Earth Sciences, Hebrew University, Givat Ram, Jerusalem, Israel.

[3]Department of Geology and Geophysics, Texas A&M University, College Station, Texas, USA.

[4]IPGS, CNRS UMR7516, Strasbourg Cedex, France.

[5]EOST, Université de Strasbourg, Strasbourg Cedex, France.

ing the general physics of pore fluid response to granular media deformation is developed, and used to study simple scenarios that lead to PP changes. We focus on the infinitely stiff end-member scenario, where granular deformation is prescribed, and the PP responds to this deformation. This end-member scenario illustrates the two possible modes of pore fluid pressurization: 1. via rapid fluid flow when fluid drainage is good, and 2. via pore volume compaction when drainage is poor. In the former case the rate of granular deformation controls PP evolution, while in the latter case fluid compressibility is found to be an important parameter and the amount of pressurization is controlled by the overall compaction. The study also predicts that shearing of over-compacted granular media may lead to significant pressurization as long as some drainage exists and a compaction phase follows dilation.

1. Introduction

Soils, unconsolidated rocks, and fault gouge may be described as porous skeletons composed of contacting grains. Often the pores are filled with fluid. The grains and the fluid form two intertwined networks: the grains connect via frictional contacts forming a heterogeneous deformable solid network, while the fluid flows in the complementary network of pores. The coupled solid-fluid system may deform in response to applied stresses, and deformation naturally arises on all time scales: from slow compaction in response to sediment load, to catastrophic failure during earthquakes and landslides. The granular network may deform elastically or through irreversible rearrangements (e.g. pore collapse). Such deformation changes the pore volume and by that affects the pore fluid pressure (PP). On the other hand, gradients in PP exert forces that may cause grains to move and the solid network to deform. The coupling between the solid matrix deformation and the value of PP is possibly the most important aspect of solid-fluid coupling: elevated PP modifies the way in which saturated granular soils and rocks respond to stresses, and often controls devastating natural phenomena such as earthquakes [e.g. *Sleep and Blanpied*, 1992], landslides [e.g. *Voight and Faust*, 1982] and soil liquefaction [*Das*, 1993; *Kramer*, 1996]. A continuum view of how PP modifies the system response to stress is formulated in the law of effective stress [*Terzaghi*, 1943]. The most important aspect of this law is the fact that the shear resistance, τ, of saturated granular material decreases linearly with increasing PP, P, since $\tau \propto \sigma - P$, where σ is the confining stress [*Terzaghi*, 1943; *Scholz*, 1990]. Therefore, the ability of saturated soils to resist shear is crucially dependent on the state of their PP: under normal conditions, when $P < \sigma$, grain-networks behave like

solids that can sustain shear stresses. However, if for some reason the PP is elevated to a level where $P = \sigma$ the shear resistance vanishes, liquefaction occurs and the grain-fluid system flows like a fluid in response to even small shear stresses. When PP within a landslide shear zone approaches the confining stress, the slide may accelerate catastrophically. When fault gouge material experience high values of PP, the dramatic reduction of shear resistance may lead to dynamic acceleration and an earthquake in response to background tectonic stresses that were previously sustained by the fault resistance to sliding. In soils, an increase in PP leading to liquefaction may cause collapse of previously supported infrastructure.

Traditionally, the mechanics of fluid-filled soils, landslides' shear zone and gouge material are studied separately. Indeed, a major difference between these three systems is their characteristic depth. While soil liquefaction is a phenomenon of the very shallow crust and is usually restricted to few tens of meters below the surface, the depth of landslides' shear zones ranges between several meters to few kilometers [e.g. *Sidle and Ochiai*, 2006], and the depth of fault gouge is restricted to the seismogenic zone, normally 2-30 km. The different depths result in differences in the effective confining stresses. This range of depth is also accompanied by a range of drainage conditions.

Despite depth and drainage differences, the basic coupled mechanics of grains and fluid may be applied similarly to soils, shear zones, and gouge layers. Indeed, the mathematical formulation that is developed here from first principles to describe PP response to granular matrix deformation is depth independent. For that reason, similar studies that are reviewed in Appendix A and deal with pore fluid pressurization for one system, may be applied also to the other systems. Therefore the term 'liquefaction' is used here to address

the general case of PP equals the confining stress, regardless of the geological setting (soil, landslides' shear zone and gouge layers). Caution should be practiced when interpreting the results, as the PP required to liquefy soils is smaller by orders of magnitude than that required to completely liquefy gouge layers. In the rest of the introduction, the importance of PP to soil liquefaction and pressurization along gouge layers is reviewed separately, but the mechanics controlling PP evolution is presented and discussed uniformly.

Soil liquefaction [*Das*, 1993; *Kramer*, 1996] is triggered by and contributes to the devastation of earthquakes, and may cause collapse of infrastructure foundations, and initiate landslides. In the process of liquefaction, external cyclic loading leading to PP rise and the consequent reduction of shear resistance causes the granular system, which under normal conditions behaves like a solid that resists shear, to flow as a fluid. As a result, liquefied soil can no longer support the infrastructure that is rooted in it and a catastrophic collapse of buildings, roads, bridges and other structures with foundations may take place (e.g., damage during earthquakes at Niigata, 1964, [*Kawakami and Asada*, 1966], or Izmit, 1999, [*Cetin et al.*, 2004]). In some earthquakes, the damage caused by liquefaction exceeds the damage by direct ground acceleration. For example, the 1995 earthquake in Kobe, Japan, caused liquefaction that resulted in more than 5500 deaths, and an estimated economic loss of over $US 130 billion [*Scawthorn and Yanev*, 1995].

Since liquefaction models are a practical necessity in geotechnical engineering, phenomenological models of coupled solid-fluid deformation have been developed (For review see [*Sawicki and Mierczynski*, 2006]). These models are usually based on continuum mixture theory formulations, and use experimental data for model calibration. A major effort to determine the mechanisms involved in earthquake-induced soil liquefaction by compar-

ing centrifuge experiment with phenomenological numerical models took place as part of the VELACS project [*Popescu and Prevost*, 1995]. None of the models accurately predict the set of experimental outcomes and by themselves show a wide and inconsistent range of predictions [*Manzari et al.*, 1994]. Recently, more sophisticated phenomenological models have improved the predictability of PP buildup and dissipation [*Zienkiewicz et al.*, 1999].

Catastrophic pore fluid pressurization may occur not only in response to cyclic loading induced by earthquakes, but also as a result of continuous shearing of fluid-filled granular layers. This is the most studied scenario for liquefaction along landslides' shear zone and fault gouge. In these cases, drainage conditions and porosity evolution were shown to control PP evolution and thus layer strength. Dynamic dilation and compaction of gouge and shear zone material are shown to be a function of shearing velocity [*Marone et al.*, 1990] and stress conditions [*Iverson et al.*, 2000; *Aharonov and Sparks*, 2002]. Dilation often leads to stable sliding as it causes PP reduction and fault hardening [*Scholz*, 1990; *Segall and Rice*, 1995; *Moore and Iverson*, 2002], while shear-enhanced compaction of under-compacted gouge may lead to extreme weakening and unstable sliding when the fault is sealed [*Blanpied et al.*, 1992]. Pore fluid pressurization and migration also control communication between fault zones and earthquakes sequencing [*Yamashita*, 1999; *Miller and Nur*, 2000].

In terms of the physics of the granular-fluid system, a matrix of granular media may deform elastically through small reversible deformation at grain contacts, and/or plastically through irreversible rearrangements (e.g. pore collapse). The term poroplasticity [*Kherbouche et al.*, 1995] is used here to describe such irreversible deformation of granular matrix in a way that modifies the shape and size of pores and the contact network between

grains, and is unrelated to microscopic dislocation glide. I.e. rearrangement takes place in the scale of an elementary grain. The traditional approach suggests that poroplasticity leads to fluid pressurization and causes liquefaction. More recently a poroelastic process was suggested to cause liquefaction in earthquakes [*Bachrach et al.*, 2001]. Sections 1.1 and 1.2 shortly review these approaches and demonstrate that a physical understanding of the mechanism by which matrix deformation generates large enough PP for soils and gouge layers to liquefy is not complete. The rheological regime that controls PP evolution, poroplasticity or poroelasticity, is still debated and so are the relevant boundary conditions (drained and undrained), and the importance of physical parameters such as fluid compressibility.

1.1. Poroplastic Approach

The poroplastic view of liquefaction relates the generation of high PP to irreversible collapse of pore volume under undrained conditions [*Sawicki and Mierczynski*, 2006]. This mechanism is supported by laboratory experiments showing that when loose sediments compact under cyclic shear [*Casagrande*, 1936; *Youd*, 1972], PP rises under undrained conditions [*Castro*, 1969]. Many models of poroplastic deformation assume specific deformation laws: in the context of soil liquefaction with deformation induced by tapping [*Snieder and van der Beukel*, 2004], in relation to crustal processes with material precipitation along pores [*Walder and Nur*, 1984], and in the context of gouge material with porosity that depends on slip [*Yamashita*, 1999] and slip velocity [*Segall and Rice*, 1995; *Samuelson et al.*, 2009].

Recently, fully coupled grain-scale models of grains and pore fluid where developed to study the relation between general deformation of granular matrix and soil liquefaction

[e.g. *El Shamy and Zeghal*, 2007; *Okada and Ochiai*, 2007; *Li et al.*, 2007]. Such models use discrete element method and are capable of simulating also irreversible grain rearrangement. Here we review two of these studies that exemplify the inconsistency in the assumed physics of soil liquefaction. (1) *El Shamy and Zeghal* [2007] study a drained system (where the fluid is allowed to flow freely out of the top boundary) with forcing induced by cyclic shear acceleration at the base of the system, and assume that pore fluid is completely incompressible, an assumption that follows many engineering interpretation of experiments [e.g. *Garga and Zhang*, 1997; *Kozlov et al.*, 1998]. (2) *Okada and Ochiai* [2007] study an undrained system (with impermeable boundaries) under forcing of contractive normal deformation, and assume a compressible pore fluid. Both studies report the generation of high enough PP for liquefaction to occur, while the latter study emphasis that high PP was generated only in initially loosely packed systems. Thus, these two works study the same problem but assume different physics (incompressible vs. compressible fluid) and different boundary conditions (drained vs. undrained). The results of *Okada and Ochiai* [2007] can be interpreted within the classical framework of soil liquefaction, as they observe high PP when compacting a loosely packed undrained granular system. However, the results of *El Shamy and Zeghal* [2007] are somewhat unexpected because they observe liquefaction under drained conditions with incompressible fluid. Indeed, a similar model that is described in *Itasca* [2005] stresses that liquefaction cannot be simulated with an incompressible fluid because then the model "does not include a mechanism for generation of pore pressure under strain". In section 5 we supply a physical explanation for this apparent violation of the classical view of liquefaction, and

show that the two models of *El Shamy and Zeghal* [2007] and *Okada and Ochiai* [2007] represent different end-members of the same physical system.

1.2. Poroelastic Approach

Poroelastic theory for coupled solid-fluid deformation [*Terzaghi*, 1943; *Biot*, 1941, 1956a, b, 1962; *Skempton*, 1960; *Wang*, 2000] assumes infinitely small reversible deformations, (an assumption better suited for rocks and cohesive matter than for granular media) and calculates solid deformation and PP. The poroelastic view attributes PP rise to the coupling between the elastic deformation of pores and the porous flow induced by the passage of P-waves [*Bachrach et al.*, 2001]. A Biot based model is developed in *Bachrach et al.* [2001], which shows that compressible fluid and low shear modulus of the granular matrix may lead to PP that exceeds the loading. A similar formulation but without inertial terms is presented in *Wang* [2000] for the general study of PP response to cyclic loading from a poroelastic point of view. It will be shown in section 3 that PP rise using this mechanism may lead to soil liquefaction only in the very top of the sediment column, and to gouge liquefaction only if the fluid was initially highly pressurized.

1.3. Overview

The diversity of models and approaches and the ongoing debates regarding the basic physics of liquefaction indicate that a coherent physical theory that explains how PP evolves in response to general deformation of the granular matrix is still missing. Such a unifying theory should be able to explain as particular cases the various field, experimental and numerical observations and the links between existing models. It should also address some basic questions that were left unanswered: What is the role of fluid compressibility

[*Garga and Zhang*, 1997]? Can liquefaction take place under drained conditions [*Das*, 1993]? And how does liquefaction occur in initially dense soils [*Soga*, 1998]?

The work presented here, aims to do exactly that. In order to achieve this goal, we first develop a general theory and then apply it within the scope of the infinite stiffness approximation, where the granular deformation is prescribed and the pore fluid responds to this deformation, without affecting solid matrix deformation. The study of this simple end-member case allows analytical solutions for the mechanics of pore fluid pressurization to be derived, compared to the numerical solutions, and highlights the mechanisms that may lead to liquefaction.

In this manuscript we develop a first principles formulation for the general PP response to granular matrix deformation in section 2. This formulation is not restricted to a particular type of deformation and may be used to study both elastic reversible processes and irreversible plastic deformation. Non-dimensional analysis of the equation that lies at the heart of the formulation reveals different physical processes that control PP evolution. The question of poroelastic vs. poroplastic rheology is discussed in section 3. Then, to study pore fluid behavior under the infinite stiffness approximation, section 4 describes the application of the formulation to a simple system of uniform grains immersed in fluid and subjected to shear loading. This application reveals the possibility of liquefaction in initially over-consolidated granular material under drained conditions. Analysis and implications are discussed in section 5, and we present our conclusions in section 6. In Appendix A we show that our formulation for the pore fluid pressure is a generalization of previous models and thus we can uncover the missing links between them. In Appendix

B we develop a general analytic solution for the basic equation that describes pore fluid pressurization.

2. Theoretical Model

In this section, first principles are used for the development of an equation describing the spatial and temporal evolution of excess pore fluid pressure in response to granular or porous matrix deformation. Let Φ be the porosity, t the time, ρ_s and ρ_f the mass densities of the bulk material of the grains and of the fluid, respectively, and $\mathbf{u_s}$ and $\mathbf{u_f}$ the grains and fluid velocities, respectively. The velocities are considered at a representative scale for the Darcy's law, i.e. they are defined for mesoscopic volumes containing at least a few grains. First, mass conservation equations are written for the grains and for the fluid:

$$\frac{\partial[(1-\Phi)\rho_s]}{\partial t} + \nabla \cdot [(1-\Phi)\rho_s \mathbf{u_s}] = 0, \tag{1}$$

$$\frac{\partial[\Phi\rho_f]}{\partial t} + \nabla \cdot [\Phi\rho_f \mathbf{u_f}] = 0, \tag{2}$$

where $\nabla\cdot$ is a divergence operator related to grains/fluid advective processes. The quantity $\Phi(\mathbf{u_f} - \mathbf{u_s})$ corresponds to the Darcy velocity [*Anghel et al.*, 2006], i.e.

$$\Phi(\mathbf{u_f} - \mathbf{u_s}) = -\frac{k}{\mu}\nabla P, \tag{3}$$

where k is the permeability, μ is the fluid viscosity and P is the excess (over hydrostatic) fluid pressure. Equation (3), Darcy's law, is derived from Stoke's equation, and is a reduced form of the momentum equation under the assumption of negligible fluid inertia. The fluid density is given by the fluid state equation:

$$\rho_f = \rho_0(1 + \beta P), \tag{4}$$

where ρ_0 is the fluid density at a reference hydrostatic pressure level, and β is the adiabatic fluid compressibility, $\beta = (1/\rho_f)(\partial\rho_f/\partial P)$. Using the adiabatic compressibility means assuming no significant heat exchange between the overpressured and underpressured zones during fast motion. We assume that grain compressibility is negligible relative to the fluid compressibility, as expected for natural sand filled with fluid such as water, so that ρ_s can be approximated as constant, and equations (1) to (4) lead to:

$$\beta\Phi\frac{\partial P}{\partial t} = \nabla\cdot[(1+\beta P)\frac{k}{\mu}\nabla P] - (1+\beta P)\nabla\cdot\mathbf{u_s} - \beta\Phi\mathbf{u_s}\cdot\nabla P. \quad (5)$$

This approach is based on the same basic principles as the approach used successfully to model instabilities in the flow of granular media and fluids [*Vinningland et al.*, 2007a, b; *Johnsen et al.*, 2006, 2007, 2008], and hydrofracture [*Flekkøy et al.*, 2002]. The value of the excess PP, P, has, for the cases considered, an upper bound set by the difference between the lithostatic and hydrostatic stresses, $\sigma_d = (\rho_s - \rho_f)gH$, where H is the depth at which matrix deformation occurs. Indeed, when $P = \sigma_d$ the effective stress vanishes, and liquefaction may occur. If P exceeds σ_d hydrofracturing is expected to take place, which is a fast transient state, not considered in this manuscript. For that reason the analysis presented here considers the case of:

$$\beta P \leq \beta\sigma_d \ll 1. \quad (6)$$

Taking fluid compressibility of $\beta = 4.5\times10^{-10}$ Pa^{-1} [*Garga and Zhang*, 1997, and reference therein], equation (6) bounds $\sigma_d \ll 2.22$ GPa and $H \ll 150$ km. This restriction on H does not limit the analysis since soil liquefaction is a phenomenon of the shallow crust, and fault gouge material is restricted by the base of the seismogenic zone. It should be noted that here we consider a single fluid with low compressibility, such as water, in the

pore space. If the pore space is filled with water/air mixture, the mixture compressibility is expected to increase significantly with respect to pure water and equation (6) might not hold. This situation is not considered in the present manuscript. Following (6), equation (5) is rewritten as

$$\beta\Phi\frac{\partial P}{\partial t} = \nabla\cdot[\frac{k}{\mu}\nabla P] - \nabla\cdot\mathbf{u_s} - \beta\Phi\mathbf{u_s}\cdot\nabla P. \tag{7}$$

The first and fourth term of equation (7) compose together the Lagrangian derivative of the PP, the second term describes PP diffusion and the third term may be viewed as the forcing.

To investigate the relative magnitude of the different terms in equation (7), a non-dimensional analysis is performed. Let us define the characteristic magnitude of the variables in the model: $P = \hat{P}/\beta$, $\mathbf{u_s} = \hat{\mathbf{u}}_\mathbf{s}u_0$, $k = \hat{k}k_0$, and $t = \hat{t}t_0$, where the $\hat{}$ notation denotes non-dimensional variables, and u_0, k_0, and t_0 are the velocity, permeability, and time scale factors, respectively. The divergence arising from equations (1) and (2) represents grain-scale rearrangements. Therefore, the derivatives in these operators are scaled by d^{-1}, a characteristic grain diameter, and $\nabla\cdot = \hat{\nabla}_1\cdot/d$. However, the gradient operator in equation (3) represents a larger length scale, over which Darcy law applies. Therefore the derivatives in this operator are scaled by l_k^{-1}, the PP diffusion length scale, and $\nabla = \hat{\nabla}_2/l_k$. l_k is bounded from the top H, and is presumably much larger than d. A natural choice for l_k is the PP skin depth $\sqrt{2Dd/u_0}$, where $D = k_0/\beta\mu\Phi$ is the PP diffusion coefficient, and $t_0^{-1} = u_0/d$ is the frequency of deformation. Assigning the non-dimensional variables in equation (7) results in:

$$\frac{\partial\hat{P}}{\partial\hat{t}} = \frac{D}{l_k u_0}\hat{\nabla}_1\cdot(\hat{k}\hat{\nabla}_2\hat{P}) - \frac{1}{\Phi}\hat{\nabla}_1\cdot\hat{\mathbf{u}}_\mathbf{s} - \frac{d}{l_k}\hat{\mathbf{u}}_\mathbf{s}\cdot\hat{\nabla}_2\hat{P}. \tag{8}$$

In this non-dimensional analysis, the forcing, third term, may be regarded as the pivot, because without this forcing, a system with an initially uniform distribution of excess PP will not evolve. Since $d/l_k \ll 1$, the fourth term (the gradient part of the Lagrangian derivative) is negligible relative to the first and third terms, and equation (8) may be rewritten as:

$$\frac{\partial \hat{P}}{\partial \hat{t}} = \frac{D}{l_k u_0}\hat{\nabla}_1 \cdot (\hat{k}\hat{\nabla}_2 \hat{P}) - \frac{1}{\Phi}\hat{\nabla}_1 \cdot \hat{\mathbf{u}}_\mathbf{s}, \tag{9}$$

where only three terms are left. In a dimensional form, equation (9) reads:

$$\frac{\partial P}{\partial t} = \frac{1}{\beta\Phi\mu}\nabla \cdot [k\nabla P] - \frac{1}{\beta\Phi}\nabla \cdot \mathbf{u}_\mathbf{s}. \tag{10}$$

The relative importance of the diffusion term, the second term in equation (10), depends on the magnitude of the coefficient $D/l_k u_0$ from equation (9), which may be interpreted as the ratio between diffusion rate D/l_k and deformation rate u_0. When $D/l_k u_0 \ll 1$, this diffusive term becomes negligible relative to the first term and the system is denoted as poorly diffusive. The dimensional excess PP may then be evaluated as:

$$P(\mathbf{x}, t) = -\frac{1}{\beta}\int_0^t \frac{\nabla \cdot \mathbf{u}_\mathbf{s}(\mathbf{x}, t')}{\Phi(\mathbf{x}, t')}\, dt', \tag{11}$$

where P depends on the fluid compressibility, β.

For $D/l_k u_0 \gg 1$, the first term of equation (10), the time dependent term, becomes negligible relative to the second diffusion term, and the system is denoted as highly diffusive. The dimensional excess PP gradient is then evaluated as:

$$\nabla \cdot [k(\mathbf{x}, t)\nabla P(\mathbf{x}, t)] = \mu\nabla \cdot \mathbf{u}_\mathbf{s}(\mathbf{x}, t), \tag{12}$$

or in the 1D case as:

$$\frac{\partial P(z, t)}{\partial z} = \frac{\mu}{k(z, t)}\mathbf{u}_\mathbf{sz}(z, t) + C(t) \tag{13}$$

where $\mathbf{u_{sz}}$ is the z component of the solid grains velocity and $C(t)$ is an integration factor. Note that equations (12) and (13) are independent of the fluid compressibility, β. This corresponds to a regime where the fluid may be considered as incompressible.

Such a non-dimensional analysis is not commonly performed in engineering applications of soil liquefaction. Instead, the time dependent term is normally neglected even when a poorly diffusive system is considered due to the small value of fluid compressibility [e.g. *Garga and Zhang*, 1997; *Kozlov et al.*, 1998]. However, in addition to the non-dimensional analysis presented above that indicates that this term should be taken into account when the PP diffusion coefficient is small enough, a simple thought experiment can demonstrate its importance: Consider a sealed system with an initial uniform distribution of pressure that is being loaded uniformly, the diffusive term in equation (10) is thus zeroed. If the time dependent term would have been neglected then equation (10) would reduce to $\nabla \cdot \mathbf{u_s} = 0$, i.e. no deformation could take place due to fluid resistivity to both flow and compression. In contrast, when the time dependent term is accounted for, it is found that the PP evolves at a rate proportional to β^{-1}, so that the small value of the compressibility leads to rapid PP elevation.

The form of the forcing term in equation (10) is intuitive in the framework of poroplasticity: when a fluid-filled granular system compacts and pore volume collapses, $\nabla \cdot \mathbf{u_s} < 0$, and the PP is expected to rise. When the system dilates, $\nabla \cdot \mathbf{u_s} > 0$, and the PP will drop. Furthermore, the form of the forcing as dependent on the local grain velocities suits a straightforward plugging of equation (10) in a model of coupled grains and fluid implemented with discrete elements method of the form of *Okada and Ochiai* [2007].

It is sometimes convenient to express the forcing term as a function of the porosity evolution rather than the divergence of the solid grains velocity. From the grains mass conservation, equation (1), it is found that

$$(1-\Phi)\nabla\cdot\mathbf{u_s} = \frac{\partial\Phi}{\partial t} + \mathbf{u_s}\cdot\nabla\Phi. \tag{14}$$

When the initial porosity and the rate of porosity evolution are assumed uniform [e.g. *Walder and Nur*, 1984; *Snieder and van der Beukel*, 2004], or when only average quantities are of interest, $\mathbf{u_s}\cdot\nabla\Phi = 0$ and $(1-\Phi)\nabla\cdot\mathbf{u_s} = \partial\Phi/\partial t$. Under these restrictions equation (10) may be rewritten as

$$\frac{\partial P}{\partial t} = \frac{1}{\beta\Phi\mu}\nabla\cdot[k\nabla P] - \frac{1}{\beta\Phi(1-\Phi)}\frac{\partial\Phi}{\partial t}. \tag{15}$$

Formulations similar to our equations (10) or (15) are found in other works dealing with the response of PP to granular and porous matrix deformation [*Walder and Nur*, 1984; *Wang*, 2000; *Samuelson et al.*, 2009], some of them specifically in the context of soil liquefaction [*Bachrach et al.*, 2001; *Snieder and van der Beukel*, 2004]. Appendix A demonstrates how these models may be directly compared to our formulation.

3. Poroelastic Pore Fluid Pressurization and Liquefaction

As the formulation presented here is not restricted to a specific rheology (poroelastic and poroplastic), the possibility of generating high enough PP for liquefaction to occur with a poroelastic mechanism is next examined. For that, we revisit a formulation developed by *Wang* [2000] describing one-dimensional spatio-temporal evolution of PP in response to temporal stressing of a fluid-filled porous material [*Wang*, 2000, equations 3.65 and 6.14]:

$$\frac{\partial P}{\partial t} = \frac{k}{\mu S}\frac{\partial^2 P}{\partial z^2} - \gamma\frac{\partial\sigma_{zz}}{\partial t}. \tag{16}$$

Where S is the uniaxial specific storage in Pa^{-1}, γ is the dimensionless loading efficiency, and σ_{zz} is the external elastic loading stress in Pa. $k/\mu S$ is a space and time constant diffusion coefficient, and $\gamma\partial\sigma_{zz}/\partial t$ is the forcing term. Equation (16) is equivalent to equation (A1) that is shown in Appendix A to be equal to our equation (10) when we assume that $\nabla \cdot \mathbf{u_s}$ occurs by elastic deformation only. Appendix A also demonstrates the equivalency between equation (16) and the formulation in *Bachrach et al.* [2001] under the assumption of negligible inertia. Thus, any conclusion drawn from this analysis applies also to the formulation discussed in section 2. Equation (16) is most suitable for investigating the poroelastic liquefaction hypothesis because its forcing term is given in the form of time dependent elastic stress loading, such as a seismic pressure wave. Indeed, *Wang* [2000] studied the behavior of equation (16) with the loading of a periodic stress wave.

Wang [2000, equation (6.57)] presented an analytical solution of equation (16) along a half space, with forcing, σ_{zz}, of the form:

$$\sigma_{zz}(0,t) = -\sigma_0 \exp(i\omega t) \tag{17}$$

where σ_0 is the amplitude of the pressure wave and ω is the loading frequency. The top of the domain is taken as drained and hence $P(z=0,t)=0$. Figure 1 shows the resultant PP magnitude, $|P|$, scaled by $\gamma\sigma_0$, as a function of the scaled depth, z/l_k. Note that the maximum value of the loading efficiency, γ, is 1. This maximum value corresponds to the case of low shear modulus for which *Bachrach et al.* [2001] find the maximum value of PP. Figure 1 and *Wang* [2000] analysis indicate that when the loading efficiency is maximal, the maximum value of PP obtained in a fluid-filled poroelastic media when a

seismic P-wave passes is bounded by $1.07\sigma_0$. That is, PP cannot exceed the stress wave amplitude by more than 7%.

For liquefaction to occur, PP must reach lithostatic values [*Sawicki and Mierczynski*, 2006]. If we consider a soil column with a thickness of 1 m, the lithostatic pressure at its base is about 25 KPa, while the hydrostatic pressure is 10 KPa. Therefore there is a need to generate excess of $P = 15$ KPa for liquefaction to occur at a depth of 1m. For the poroelastic liquefaction to occur, the forcing magnitude then must be 14 KPa, two orders of magnitude larger than typical amplitudes of seismic pressure waves [*Bachrach et al.*, 2001]. If we consider a fault gouge at depth of 15 km, the excess PP needed for complete liquefaction is about 0.2 GPa. The excess PP generated by the poroelastic mechanism with a forcing wave of 100 Pa (typical value for seismic pressure wave) is a negligible fraction of the needed value. These simple examples indicate that the poroelastic mechanism is applicable only for the top few centimeters of the grains-fluid column, or when PP is initially very close to lithostatic values. Therefore, in the next section we turn back to study the classical poroplastic volume collapse mechanism using a simple prescribed plastic matrix deformation model.

4. The Infinite Stiffness Approximation

The formulation presented so far is applicable to a general fully coupled system. But in order to actually solve the fully coupled system, another equation for the evolution of the solid grains velocity needs to be prescribed. In this equation PP gradients act as a force on the granular matrix directed toward the lower fluid pressure [e.g. *McNamara et al.*, 2000]. Such forces are sometimes referred to as seepage forces [*Mourgues and Cobbold*, 2003; *Rozhko et al.*, 2007]. However, here we first solve a simpler scenario - the

infinitely stiff system, which means that the matrix deformation is externally prescribed and the PP responds to this deformation. The reason we do not immediately solve also the other direction of the deformation of the solid matrix in response to PP gradients, is because currently there is no first principles based theory that predicts the general (elastic and plastic) granular matrix deformation induced by a PP field that varies spatially and temporally. Moreover, currently there is not even a first principles based theory that predicts the deformational response of a dry granular matrix to general loading [*Forterre and Pouliquen*, 2008]. To overcome this limitation, previous works that solve for the fully coupled system with a continuum approach use phenomenological relations to describe the porosity evolution in response to external loading and PP variations [e.g. *Snieder and van der Beukel*, 2004; *Samuelson et al.*, 2009]. Consequently they are restricted to a specific type of deformation, material properties and boundary conditions. It is proposed that a general solution for the effect of PP variation on the matrix deformation, and thus a fully coupled solution for the general deformation of grains-fluid system may be achieved in the framework of a granular dynamics algorithm [e.g. *McNamara et al.*, 2000; *El Shamy and Zeghal*, 2007; *Okada and Ochiai*, 2007].

In the infinite stiffness approximation presented here, local pore volume collapse is externally prescribed and is characterized by $\nabla \cdot \mathbf{u_s} < 0$ in equation (10) or $\dot{\Phi} < 0$ in equation (15), which leads to pore fluid pressurization and to the generation of PP gradients and seepage forces. In a fully coupled formulation the pressure gradients will oppose the pore collapse deformation and will act to push the pore walls aside and somewhat relax the source of pressurization. For that reason the maximum PP within a fully coupled system is limited by the order of magnitude of the confining stress that drives pore volume

change. In that sense the resultant absolute value of the PP achieved under the infinite stiffness approximation serves as an upper bound with respect to a fully coupled system.

4.1. Application to Shearing of Fluid-Filled Uniform Granular System

Here we explore the physical behavior of equation (10) under poroplastic conditions. This exploration is a first step in mapping the conditions that will cause liquefaction by irreversible pore volume collapse during shear of a granular system. For that, a simple system of hexagonally packed uniform grains immersed in fluid is studied (Figure 2). The top boundary is subjected to a constant shear velocity, V_{sh}, in the x direction. The system is assumed to respond in localized shear deformation along one row of grains (Figure 4a, sliding row in yellow). Along the x direction the system is assumed periodic and hence the divergence of the velocity is reduced to $\nabla \cdot \mathbf{u_s} = \partial \mathbf{u_{sz}}/\partial z$, and the problem becomes one dimensional. The porosity, Φ, and the granular velocity perpendicular to the shear direction, $\mathbf{u_{sz}}$, of the sliding row of grains are functions of time, t (and thus of displacement, x) (Figure 3):

$$\begin{aligned} \mathbf{u_{sz}} &= V_{sh}\frac{[\cos(\pi/3) - V_{sh}t'/d]}{A} \\ \Phi &= 1 - \frac{\pi}{4A} \\ A &= \sqrt{1 - [\cos(\pi/3) - V_{sh}t'/d]^2}. \end{aligned} \tag{18}$$

where $t' = (t + x'/V_{sh}) \bmod (d/V_{sh})$, and x' depends on the initial conditions as explained below.

The simulated domain of thickness h is assumed to be buried at depth H (where $h \leq H$), so that excess PP of $P = \sigma_d$ is interpreted as resulting in zero effective stress and the onset of liquefaction. The shearing row is located at distance $\zeta = h/2$ from the boundaries of the

system. Three scenarios are tested. In the first two cases, $\zeta \ll l_k$, so that the grains pack has a vertical dimension smaller than the PP skin depth, l_k: In a drained system, denoted as B.C. of type 1, a constant PP of $P = 0$ is assumed at the top of the system as if an open fracture drains the buried domain at its top. In an undrained system, denoted as B.C. of type 2, zero fluid flux across the top boundary is assumed, simulating an impermeable layer that lies on top of the domain. In these two cases the bottom boundary is assumed undrained. In the third case, a large system is considered where $\zeta \gg l_k$, denoted as B.C. of type 3, to allow the development of a full diffusion profile. In this case, the exact details of the prescribe boundary conditions have only minor importance as the advancing PP diffusion front does not reach the boundaries in the studied time scale. Table 1 summarizes the parameters used in the simulations.

Two types of initial conditions are studied: In the first, denoted here as dense packing, the sliding row is initially in a hexagonal configuration (Figure 4a, sliding row in yellow), and $x' = 0$. In this case, sliding is accompanied by initial dilation until a cubic configuration is reached along the sliding row. Then, the system compacts until hexagonal packing is reached again. A full period is the duration between two consecutive hexagonal configurations. In the second initial condition, termed here loose packing, the sliding row is placed in a cubic configuration with respect to the row below it (Figure 7a), and $x' = 0.5d$. In this case, the system first compacts to a full hexagonal configuration and then dilation along the sliding row brings it back to a cubic configuration. Here a full period is the duration between two consecutive cubic configurations.

The set of equations (10) and (18) together with Carman-Kozeny equation (Table 1) for the relation between porosity and permeability are solved numerically using a 1D Crank-Nicholson scheme.

4.1.1. Dense Packing

First, the case of dense initial grain packing is studied, i.e. all rows are hexagonally packed.

Drained system: Simulation results show that when the system is drained (B.C. of type 1), the excess PP, initially taken as zero, becomes negative when the system starts to dilate as it shears (Figure 4b, red curve). As deformation continues, fluid influx from the top boundary, driven by the pressure gradient that forms between the top of the domain and the location of deformation, decreases the magnitude of this negative value. When a cubic configuration is reached, i.e. the system has slid to its maximal porosity, PP is zero again. During compaction, PP rises until it gets to its maximal value when the system is back in hexagonal packing.

The parameters of Table 1 imposes a highly diffusive regime, and the proximity of the drained boundary to the shearing row, $\zeta \ll l_k$, allows good drainage. Therefore, PP evolution is described by equation (13). The pressure gradient may then be estimated as $\partial P/\partial z = -P/\zeta$, and the PP along the sliding row is evaluated as:

$$P = -\frac{\mu\zeta}{k}\mathbf{u_{sz}}, \tag{19}$$

The PP evolution according to equation (19) is compared to the numerical solution (Figure 4b, dashed turquoise curve), where the permeability $k = k_{min}$ is taken as the permeability resulting from the porosity of the hexagonal packing that is constantly preserved in this

example, on top of the sliding row. Excluding the very onset of the motion that is governed by the time dependent term of equation (10), the analytical and numerical solutions match.

Equation (19) reveals that in the drained case the value of the PP along the shearing row depends linearly on the fluid viscosity, μ, the distance to drainage, ζ, and on the inverse of the permeability k^{-1}. For Carman-Kozeny law (Table 1), $k = k(d^2)$, and thus $P \propto d^{-2}$. All these dependencies, together with fluid compressibility independency, were verified in a parameters sensitivity study.

When accounting for the relations in equation (18), another dependency may be established. The maximum value for the PP, P_{max} is attained at the end of the period, when $t' = d/V_{sh}$. Assigning this value of t' in equation (18), it is found that $\mathbf{u_{sz}}(t' = d/V_{sh}) = -V_{sh}/\sqrt{3}$. Combining this results with equation (19) predicts a linear relation between P_{max} and shear velocity, V_{sh}, as depicted in Figure 5.

Undrained system: For an undrained system (B.C. of type 2), the excess PP becomes increasingly negative during dilation and returns to zero when the system compacts again (Figure 4c). This occurs because during dilation the pore volume expands and $\nabla \cdot \mathbf{u_s} > 0$. With no fluid supply from the boundaries, the average PP must decrease. During compaction $\nabla \cdot \mathbf{u_s} < 0$ and PP increases back to the initial zero value. The excess PP is negative throughout this simulation so that overpressure is not generated. We derive an analytic solution for the undrained case when loose packing is considered below.

Large system: The third scenario of a large system with $\zeta \gg l_k$ (B.C. of type 3) shows PP evolution that is a combination of the drained and the undrained regimes (Figure 4d, purple curve). Initially PP evolves similarly to an undrained system. However, the effect of fluid flow oriented towards the shearing row compensates for the negative value, so that

minimum PP is attained before cubic packing, and PP increases to positive value at the end of the period similar to a drained system.

It is possible to derive an analytic solution for the case of large systems assuming the diffusion coefficient is constant with time i.e. $D = D_c = k_{min}/\beta\mu\Phi_{min}$. Appendix B shows this derivation and figure 6 presents the comparison between the analytic solution and simulation conducted with the imposed constant diffusion coefficient D_c along the shearing row. The analytic prediction reveals that the characteristic pressure scale for the evolving PP may be expressed as $d/\beta\sqrt{\pi D_c t_0}$. For the parameters of Table 1 this scale is $\sim$1.5 MPa, which is the order of PP magnitude that is found in figure 6.

4.1.2. Loose Packing

Next, initially loose packing systems are sheared. During the first half of the period, for all boundary conditions, the system compacts and PP increases. Maximum values are attained in the middle of the period when the systems are in hexagonal configuration. We next review the systems behavior during the second half of the period, when they dilate back to cubic packing.

Drained system: When a drained system starts dilating in the second half of the period, PP first drops to a negative value and then rises back to zero due to fluid influx from the boundary (Figure 7b). Again, linear relation (with opposite signs) between $\mathbf{u_{sz}}$ (Figure 7a, green curve) and P (Figure 7b) following equation (19) is observed.

Undrained system: For the undrained system, in the second half of the period, when dilation starts, PP returns to zero from its maximal value (Figure 7c, black curve). Here, excess PP is positive throughout the simulation. In this case of undrained boundary and $\zeta \ll l_k$, PP diffuses only inside the small system but there is no inflow and outflow to

and from the domain. As a result, the diffusive term of equation (10) becomes negligible when evaluating the total excess PP within the domain. Thus, the system should follow equation (11) as if it is poorly diffusive. Evaluating $\nabla \cdot \mathbf{u}$ as $\mathbf{u_{sz}}/d$ and assigning the expressions for $\mathbf{u_{sz}}$ and Φ from equation (18):

$$P = -\frac{1}{\beta}\left\{\frac{\pi}{4}\ln\left[\frac{\pi - 4A}{\pi - 4}\right] + A - 1\right\} \tag{20}$$

$$A = \sqrt{1 - [\cos(\pi/3) - V_{sh}t'/d]^2}.$$

Comparison between equation (20) and the numerical solution assuming PP does not diffuse away from the shearing row (by setting the permeability to zero) shows good fit (Figure 7c, inset). Equation (20) indicates that in the lack of PP diffusion, P is independent of shearing velocity, V_{sh}, but is a function of the inverse fluid compressibility, β^{-1}. The smaller is β, the larger will be the PP along the domain.

Large system: A large system with $\zeta \gg l_k$ shows that in the second half of the period, upon dilation, PP decreases to a negative value, but the period ends with an increasing trend (Figure 7d). The overall evolution of PP is a combination of the drained and the undrained regimes, with minimum PP occurring not immediately upon dilation initiation like in a drained system and not at the end of the period like in an undrained system, but in between. This is the effect of competition between depressurization resulting from the time dependent term of equation (10) and fluid inflow originating from the diffusion term of equation (10).

4.1.3. Results

This analysis indicates that when the system is undrained with $\zeta \ll l_k$ (B.C. of type 2) shearing of initially dense granular material generates only negative excess PP. When an initially loose configuration is sheared, pore fluid is pressurized and reaches 0.16 GPa,

a value corresponding to σ_d at depth of 10 km, or alternatively, a value that reduces the effective stress along gouge material buried at depth of 15 km by more than 70%. It should be remembered that under the infinite stiffness approximation used here, we do not prescribe a confining stress, and the value of PP is not limited, but it is simply a function of the overall pore volume strain. In this framework, soil liquefaction at shallower depth will take place earlier in the period. For example, reaching $P = \sigma_d$ at a depth of 10 m requires the generation of excess PP of 0.15 MPa that occurs after 1% of a period ($t = 0.01d/V_{sh}$). When the infinite stiffness assumption is relaxed, the value of maximum PP is expected to be bounded by the order of magnitude of the confining stress because PP gradients between the system interior and exterior will act to oppose further pore volume compaction and limit pressurization to the exact value that dynamically balances the forces acting to compact pore volume.

When some drainage exists (B.C. of types 1 and 3) pore fluid pressurization (to positive values) occurs even when the granular matrix is initially dense or over-consolidated, as is called in soil mechanics. For the completely drained system (B.C. of type 1) excess PP becomes positive simultaneously with the initiation of compaction, and reaches a maximum of 0.21 MPa (for Table 1 parameters) corresponding to the effective normal stress at depth of 14 m. For a large system (with $\zeta \gg l_k$), B.C. of type 3, PP becomes positive after some delay from the onset of compaction, and reaches a maximum of 3.3 MPa (for dense packing) at the end of the second period, corresponding to the effective stress at great depth of 220 m. In these cases pore fluid pressurization occurs even for initially dense systems as long as there is a compaction phase that follows the dilation.

5. Discussion

This section discusses the physics of PP evolution is response to granular matrix deformation that arises from our theoretical formulation. We also discuss the implications of this physics to numerical, experimental and natural systems. First, we consider the mechanisms that control changes in PP based on the formulation presented in section 2. The basic equations for the PP evolution, equations (10) and (15), predict two different physical mechanisms that compete in controlling the evolution of PP, but their relative contribution is determined by the parameters and boundary conditions of the system. The two mechanisms are $\mathcal{A}$ - pressurization and depressurization induced by changes of pore volume (equation (11)) , and $\mathcal{B}$ - pressurization and depressurization induced by Darcy flow (by equations (12) and (13)).

In mechanism $\mathcal{A}$, pore fluid that is isolated and trapped within a shrinking pore volume is pressurized, while pore fluid isolated and trapped in expanding pore volume is depressurized. The magnitude of pressurization and depressurization is controlled by the fluid compressibility, and by the overall pore volume change that is expressed by $\int_0^t \nabla \cdot \mathbf{u_s}(\mathbf{x}, t')\, dt'$ in equation (11). In that sense this mechanism holds memory of previous states of porosity.

The second mechanism, $\mathcal{B}$, is less intuitive. Because of mass conservation, convergence (or divergence) of grains causes the pore fluid that resides between the grains to flows out of (or into) this region. Because porous flow obeys Darcy's law, pressure gradients arise between the location of converging (or diverging) grains and the surrounding, to generate these flows. Here, PP evolves from the arising pressure gradients. The magnitude of the generated pressure gradient depends on the rate of grains convergence or divergence, as

574 expressed by $\mathbf{u_{sz}}$ in equation (13). This mechanism holds no a memory of previous states
575 of porosity but pressurization depends on the instantaneous rate of pore deformation. PP
576 evolution due to Darcy flow is normally not considered to cause liquefaction, although
577 it may lead to significant pressurization. Moreover, because of its 'lack of memory', this
578 mechanism may lead to generation of high PP even when an initially dense granular matrix
579 is sheared. Indeed, upon shearing an over-compacted layer, it will first dilate, and then
580 oscillate around its critical porosity [*Aharonov and Sparks*, 2002; *Gabet and Mudd*, 2006].
581 In the oscillatory stage, any compaction phase, with $\nabla \cdot \mathbf{u_s} < 0$, will lead to pressurization
582 despite the fact that the instantaneous porosity may be significantly larger than the initial
583 porosity.

584 The relative importance of the two pressurization mechanisms depends on both the
585 internal properties of the system and the boundary conditions that may have different
586 characteristics, such as a strong contrast between internal and boundary permeabilities.
587 In order to account for the internal properties we define the diffusion number [*Samuelson*
588 *et al.*, 2009] that expresses the competition between two rates: The rate of pore pressure
589 diffusion, D/l_k, where $l_k = \sqrt{2Dd/u_0}$ is the PP skin depth, and the rate of deformation,
590 u_0. The ratio of these two rates that appears as the coefficient of the second term in
591 equation (9), determines whether pore fluid is effectively trapped within a shrinking or
592 expanding pore volume, or whether it may flow freely. When $D/l_k u_0 \ll 1$, the system is
593 defined as poorly diffusive because PP cannot diffuse away or into a deforming pore volume
594 during the time scale of deformation. When $D/l_k u_0 \gg 1$, the system is defined as highly
595 diffusive because PP can diffuse freely within the time scale of pore deformation. The
596 drainage boundary conditions of the system are independent of the diffusion number. If we

consider only the two end-members of completely drained boundaries that are connected to a constant pressure reservoir and completely undrained boundaries that prevent fluid inflow and outflow, then all four combinations of highly diffusive and poorly diffusive systems with drained and undrained boundaries are possible.

We present here a simple three stages scheme that determines what will be the dominant mechanism for PP evolution, based on the diffusion number, drainage boundary conditions and system size. 1) Evaluate the diffusion number. If the system is poorly diffusive ($D/l_k u_0 \ll 1$), then mechanism $\mathcal{A}$ of PP evolution due to changes in pore volume will dominate regardless of the boundary conditions. If $D/l_k u_0 \gg 1$, there is a need to move to the next stage. 2) Evaluate the ratio of the distance between the deforming zone and the boundary, ζ, to the PP skin depth, l_k. If $\zeta/l_k \gg 1$, the system is large and both mechanisms of PP evolution, $\mathcal{A}$ and $\mathcal{B}$, operate together (like the large system scenario, B.C. of type 3, that is tested in section 4.1). If $\zeta/l_k \ll 1$, there is a need to move to the next stage. 3) Evaluate the drainage boundary conditions. If they are drained then the dominant mechanism is $\mathcal{B}$, PP evolution due to Darcy flow (like B.C. of type 1). If they are undrained then mechanism $\mathcal{A}$ will dominate (like B.C. of type 2).

In this scheme, the last situation of a small, highly diffusive system, with undrained boundary conditions is probably the most puzzling. In such a case, when the system undergoes compaction or dilation, pore fluid cannot flow away or into the system, so despite the fact that PP can quickly equilibrate within the system because it is highly diffusive, the evolution of the average PP will follow mechanism $\mathcal{A}$. Next in the discussion we apply this scheme to numerical, experimental and natural systems.

5.1. Applications to Grains and Pore Fluid Modeling and Experiments

When modeling a finite system of grains and fluid, the system parameters, size and boundary conditions are determined in advance. If the system is small ($\zeta/l_k \ll 1$) and undrained (B.C. of types 2), PP diffusion between the system and the surrounding is prohibited, and mechanism $\mathcal{A}$, pressurization by changes in pore volume will dominate. Therefore, fluid compressibility must be accounted for, but diffusive effects may be neglected, and the relevant equation to solve is (11). Pore fluid pressurization is expected only if the system is compacting with respect to its initial porosity, and the magnitude of PP is proportional to the inverse of fluid compressibility.

When modeling a small drained system (B.C. of type 1) the process of PP diffusion becomes crucial, and pressure gradients arise between the system interior and the boundaries (that are kept at some constant pressure). The dominant PP evolution mechanism will be $\mathcal{B}$, Darcy pressurization. Accounting for fluid compressibility will only introduce a short lived transient effect, and if this effect is not of interest it is sufficient to solve Laplace equation (12). Pore fluid pressurization is expected when the system compacts rapidly enough with respect to any former state and not necessarily with respect to the initial state. Generated PP is linearly proportional to the compaction rate, fluid viscosity, distance to drainage, and the inverse of permeability.

When modeling a large system, (B.C. of type 3), the drainage conditions along the boundaries do not dictate the system dynamics and both pressurization mechanisms, $\mathcal{A}$ and $\mathcal{B}$. In this case, both the diffusive term and the time dependent term with fluid compressibility should be accounted for, and the full fluid equation (10) should be solved.

We may now turn to analyze the two numerical models of *El Shamy and Zeghal* [2007] and *Okada and Ochiai* [2007] that are presented in section 1.1. *El Shamy and Zeghal* [2007] report the occurrence of liquefaction under drained conditions and with incompressible fluid. Liquefaction starts at the top of the grains column, close to the drained boundary. Such conditions lead to pressurization by mechanism $\mathcal{B}$ due to Darcy flow. *Okada and Ochiai* [2007] report the occurrence of liquefaction when compacting loose, undrained system with compressible fluid. Such conditions lead to pressurization by mechanism $\mathcal{A}$ due to pore volume compaction. Thus, these two models simulate the two end-member mechanisms that are included in equation (10).

Interpretation of experimental results should follow a similar scheme. *Samuelson et al.* [2009] perform an experimental series of shearing fluid-filled granular material using a triaxial pressure vessel in a double direct shear configuration. We briefly revisit here their system, in order to demonstrate the applicability of our analysis to experiments. The parameters in the experimental system are: $\zeta = 2 \times 10^{-3}$ m, $d = 1.27 \times 10^{-4}$ m, $u_0 = 10^{-6} - 10^{-4}$ m/s, $\Phi = 0.2$, and $k = 4.2 \times 10^{-14}$ m^2. PP was kept constant on the boundaries. This combination of parameters leads to a drained, small ($\zeta/l_k \ll 1$), and highly diffusive ($D/l_k u_0 \gg 1$) system, and as a result negative PP cannot be sustained after the onset of dilation. Indeed, *Samuelson et al.* [2009] report that upon dilation no hardening is observed because fluid inflow immediately compensates for the newly generated pore space.

5.2. Application to Natural Systems

The scheme presented above may also be used to analyze the mechanics of PP evolution for field cases. One should evaluate the diffusion number of the system, determine the location and type of its boundaries, and the system size.

5.2.1. Liquefaction of Shear Zones

As a first natural system we consider shear zones that accommodate long shear strain, similar to the uniform grain system that is studied in section 4.1. Critical state theory predicts and experiments have shown that during shear, loose soils contract while dense soils dilate [*Casagrande*, 1936]. Invoking this theory to explain liquefaction of shear zones leads to the conclusion that while loosely packed shear zones may liquefy due to grain collapse leading to PP increase and the reduction of frictional resistance, dense shear zones inhibit liquefaction as they do not allow pore fluid to be pressurized [*Iverson et al.*, 2000]. Indeed, if the shear zone of a landslide is confined by impermeable barriers, then the PP evolution within it will follow mechanism $\mathcal{A}$. In that case, only initially loose shear zones may become pressurized enough to facilitate mobilization of a landslide into debris flow.

However, in many cases, the shear motion at the base of landslides and also during earthquakes is large enough for the shear zone to reach its critical porosity [*Iverson*, 2005]. That is, an over-compacted shear zone will first dilate, and then after the first several centimeters to several meters [*Iverson*, 2005; *Garagash and Rudnicki*, 2003] it will oscillate around some steady state porosity. Such oscillations include also compacting phases, not with respect to the initial over-compacted configuration, but with respect to the critical porosity. If the shear zone is well drained, then mechanism $\mathcal{B}$ of pressurization by Darcy flow may operate, causing significant pressurization, and potentially leading to

acceleration of shear. *Gabet and Mudd* [2006] report on debris flows mobilization from dense soils, and find correlation between mobilization and fines/sand ratio, where soils with a small ratio are mobilized. Following the analysis presented here, it is suggested that small fines/sand ratio contributes to good drainage of the shear zone, due to the larger fraction of large sand particles. Thus, any short compactive stage that followed the initial dilative phase, a scenario that is reviewed in *Gabet and Mudd* [2006], may lead to pressurization by mechanism $\mathcal{B}$ due to Darcy flow, and thus will generate an accelerating debris flow. In fact, since most shear zones are initially over-compacted, we consider this mechanism to dominate.

5.2.2. Soil Liquefaction

Next we address the mechanism of PP evolution during soil liquefaction. The classical view of soil liquefaction attributes the rise of PP to cyclic strain forcing of the soil skeleton [*Sawicki and Mierczynski*, 2006]. The formulation developed in section 2 is general and does not assume specific forcing, but the analysis of shearing uniform grain system presented in section 4.1 is built upon continuous shearing. We claim here that if the cyclic strain is large enough to allow both dilation and compaction of a single grain (shear strain $\geq$ grain radius), then the behavior observed for continuous shearing is analogous to cyclic shearing. Still, positive PP may evolve only if the soil experiences some compaction during its deformation, but whether compaction actually occurs and its magnitude depend strongly on its initial porosity and on the duration of the applied force, that are beyond the scope of this paper. Here we study the mechanisms by which PP may evolve given an optimal deformation of the soil skeleton.

We start analyzing the conditions and mechanisms for soil liquefaction induced by the passage of seismic shear waves by choosing a set of typical parameters. We account for pore water and use water compressibility and viscosity from Table 1. The porosity is taken to be $\Phi = 0.46$, that corresponds to medium void ratio for 3D packing of spheres [*Okada and Ochiai*, 2007]. We analyze the situations of medium sand and of silt with grain diameter of $d = 5\times10^{-4}$ and 5×10^{-5} m, respectively, and corresponding permeabilities of $k = 10^{-10}$ and 10^{-14} m^2. These permeabilities are smaller than predicted by Carman-Kozeny (in particular for the silt) as it is assumed that grain size is not completely uniform. The velocity of deformation is taken to be the peak ground velocity (PGV) induced by the seismic waves. We use $u_0 = 0.1$ m/s that is estimated to be the minimal PGV that induce liquefaction [*Kostadinov and Towhata*, 2002]. For these parameters, the PP skin depth and diffusion number are $l_k = 2.2$ m and $D/l_k u_0 \sim 2000$ for the sand and $l_k = 6.9\times10^{-3}$ m and $D/l_k u_0 \sim 70$ for the silt, so that for both soil types the system is highly diffusive. If we consider that the source of liquefaction lies at a depth of 5 m, and this is also the distance to the drained boundary, ζ, then for both the medium sand and for the silt, $\zeta/l_k > 1$, and the system is large. Following the scheme presented above, both mechanisms of PP evolution, $\mathcal{A}$ and $\mathcal{B}$, should be considered. Due to the large diffusion number, mechanism $\mathcal{B}$ of PP evolution by Darcy flow is expected to be more significant, similar to the results of the large system (B.C. of type 3) that was analyzed in section 4.1.

Larger permeability and smaller PGV will lead to larger l_k and larger diffusion number, and will cause mechanism $\mathcal{B}$ to be even more dominant. However, such conditions are also expected to decrease the magnitude of the evolving PP because with accordance to equation (19) evolving PP depends linearly on the PGV, and on the inverse of the

permeability. For example, if the permeability of the medium sand is as large as $k = 10^{-9}\text{m}^2$, and the PGV is $u_0 = 0.01$ m/s, then $l_k = 22$ m is much larger than ζ. In such a case only Darcy pressurization (mechanism $\mathcal{B}$) will be of importance, and the maximum PP, according to equation (19) is 0.05 MPa, while the excess PP needed for liquefaction at depth of 5 m is 0.075 MPa.

Smaller permeability and larger peak ground velocity will cause the diffusion number to be much smaller, leading to dominance of mechanism $\mathcal{A}$. However, for the system to be strictly in the poorly diffusive regime, and accounting for PGV of 0.1 m/s, the medium sand permeability needs to be smaller than 2×10^{-17} m^2, which is significantly smaller than expected for natural sands.

This simple analysis shows that the process of soil liquefaction is similar to the large system (B.C. of type 3) studied in section 4.1, and that both mechanisms of PP evolution may operate together. Because the diffusion number is large, positive PP may evolve even if the soil is not strictly compactive, as long as some transient compaction occurs, similar to the case studied in Figure 7d.

5.2.3. Nucleation of Motion Along Faults

Finally in the discussion we address the evolution of PP during the stage of sliding nucleation along fault zones. Many fault zone systems are characterized by strong permeability contrast between the gouge material and the confining blocks, so that the gouge layer may be considered as the granular system while the confining blocks impose the drainage boundary conditions. We consider here a well-compacted thin gouge layer of thickness, 2ζ, of several centimeter. For the nucleation stage we consider a tectonic rate of deformation, $u_0 = 10^{-10}$ m/s. For the medium sand and silt, the small deformation

rate leads to $\zeta/l_k \ll 1$, and to a very large diffusion number. Even for clay size gouge with $d = 10^{-6}$ m and permeability of $k = 10^{-19}$ m^2, $\zeta/l_k < 1$ and $D/l_k u_0 >> 1$, so that the granular layer is small with respect to the PP skin depth, and the system is highly diffusive. According to the scheme presented above, the boundary conditions imposed by the confining blocks determine the mechanism of PP evolution. If the confining blocks are impermeable, the PP will evolve following mechanism $\mathcal{A}$ according to changes of pore volume, and negative excess PP will evolve in response to any dilation, resulting in dilatancy hardening. If the confining blocks are highly fractured and allow for communication with a constant pressure reservoir then the PP will evolve following mechanism $\mathcal{B}$, due to Darcy flow, fluid inflow will compensate for the newly generated pore volume, and hardening will not be observed [*Samuelson et al.*, 2009].

6. Conclusions

This manuscript presents a formulation describing pore fluid pressurization and flow in response to general granular matrix deformation, and is thus applicable to both elastic reversible deformation and to large scale irreversible deformation. The formulation is used to examine the conditions and processes by which pore fluid pressure evolves to large enough values that may lead to liquefaction of soils and shear zones.

It is found that the relative degree of drainage expressed by the ratio between fluid diffusion and granular deformation rates, $D/l_k u_0$, and by the boundary conditions is of great importance. When the ratio $D/l_k u_0$ is small (for example, when the permeability is small), or the boundaries are undrained, pore fluid pressurization occurs only for initially loose granular matrices and is highly dependent on fluid compressibility, with faster pressurization for smaller compressibility. Under such conditions pressurization is

not correlated to the rate of deformation but to overall volumetric compaction. When the ratio $D/l_k u_0$ is large, or when the boundaries are drained pore fluid pressurization occurs also in initially dense granular matrices during any later compaction stage that follows dilation. Here, PP depends on the compaction velocity, fluid viscosity, system permeability and distance to drainage, but is independent of fluid compressibility. This regime may explain liquefaction phenomena in initially dense and well drained soils and shear zones, conditions that were previously thought to be liquefaction resistant despite field evidences showing otherwise [e.g *Soga*, 1998; *Gabet and Mudd*, 2006]. For large system with dimensions that exceed the PP skin depth both fluid compressibility and the rate of deformation control fluid pressurization.

Appendix A: Comparison with Other Models

Here, our equations (10) and (15) is compared to other models studying the response of PP to granular or porous matrix deformation. To facilitate comparison, the notation of this manuscript is adopted where possible.

A1. Elastic Formulations

Wang [2000] presents two equivalent poroelastic formulations for the temporal and spatial evolution of PP in response to elastic forcing in a fluid-filled porous material. The first formulation describes the forcing as a temporal evolution of stress and is presented in equation (16). The second formulation describes the forcing in terms of temporal evolution of strain:

$$\frac{\partial P}{\partial t} = \frac{kM}{\mu}\frac{\partial^2 P}{\partial z^2} - \alpha M \frac{\partial \epsilon_{zz}}{\partial t} \tag{A1}$$

Equation (A1) follows *Wang* [2000, equation (6.18)] with notation simplification following *Wang* [2000, equations (3.37) and (3.64)]. Where M is Biot's Modulus and α is Biot-Willis coefficient. When grains are assumed incompressible, $M = 1/\beta\Phi$ and $\alpha = 1$ [*Wang*, 2000, table 3.2]. Therefore equation (A1) may be rewritten as:

$$\frac{\partial P}{\partial t} = \frac{k}{\mu\beta\Phi}\frac{\partial^2 P}{\partial z^2} - \frac{1}{\beta\Phi}\frac{\partial \epsilon_{zz}}{\partial t} \tag{A2}$$

This form is equivalent to our equation (10), since the forcing term $\partial\epsilon_{zz}/\partial t$, representing the one dimensional strain rate, may be rewritten as $\partial \mathbf{u_{sz}}/\partial z$. For example, for a periodic strain of the form $\epsilon_{zz} = \epsilon_0 \exp(i\omega t)$, the corresponding grains velocity will be $\mathbf{u_{sz}} = \int_z (\partial\epsilon_{zz}/\partial t)dz = i\epsilon_0\omega z \exp(i\omega t)$. It is a surprising result that equation (A2) that was developed from a purely elastic point of view, is in fact equivalent to our equation (10) which did not assume elasticity. The only difference is *Wang* [2000] assumption of uniform permeability in the diffusion term (first term on the righthand side) of equation (A2), which does not necessarily hold for the general formulation of equation (10).

Bachrach et al. [2001] present a study of the propagation of pressure waves in a poro-elastic material induced by stress forcing using Biot's equations. Next, the equivalency between *Bachrach et al.* [2001] formulation and equation (16) (which follows *Wang* [2000, equation (6.14)]) is demonstrated under the assumption of negligible inertia, an assumption that is discussed in the following. Combining *Bachrach et al.* [2001, equation (7) and equation (11)] and neglecting inertial terms, it is found that:

$$\frac{\partial P}{\partial t} = \frac{k}{\mu} 2D \left(1 - \alpha\frac{2\alpha F}{H}\right)\frac{\partial^2 P}{\partial z^2} - \frac{2\alpha D}{H}\frac{\partial \sigma}{\partial t} \tag{A3}$$

As before, $\alpha = 1$, is the Biot-Willis coefficient for incompressible grains. $D = (2\beta\Phi)^{-1}$ and $H = K_\nu^{(u)} = K_\nu + (\beta\Phi)^{-1}$, where $K_\nu^{(u)}$ and K_ν are the undrained and drained uniaxial bulk

moduli, respectively. H and D are resolved following their definition in *Bachrach et al.* [2001] and under the assumption of incompressible solid grains. Assigning the expressions for α, H and D into equation (A3) results in:

$$\frac{\partial P}{\partial t} = \frac{k}{\mu}\frac{1}{\beta\Phi + K_\nu^{-1}}\frac{\partial^2 P}{\partial z^2} - \frac{1}{K_\nu^{(u)}\beta\Phi}\frac{\partial \sigma}{\partial t}. \tag{A4}$$

Following [*Wang*, 2000, equation (3.52)], $\beta\Phi + K_\nu^{-1} = S$, and following [*Wang*, 2000, equation (3.85) and table 3.2], $(K_\nu^{(u)}\beta\Phi)^{-1} = \gamma$. Thus it is proven that equation (A4) (which is an inertia free version of Biot's equations, as expressed in *Bachrach et al.* [2001, equations (7) and (11)]) is identical to *Wang* [2000, equations (6.14)] and to equation (16).

Next, we wish to determine the limits for the validity of our assumption of negligible inertia. For that, *Bachrach et al.* [2001, equations (7) and (11)] are reviewed:

$$\begin{aligned} \rho_b\frac{\partial^2 v}{\partial t^2} + \rho_f\frac{\partial^2 w}{\partial t^2} &= \frac{\partial \sigma}{\partial z} \\ \rho_f\frac{\partial^2 v}{\partial t^2} + m\frac{\partial^2 w}{\partial t^2} &= \frac{\partial P}{\partial z} + \frac{\mu}{k}\frac{\partial w}{\partial t}, \end{aligned} \tag{A5}$$

where ρ_b is the density of the fluid-filled porous material, m is a coupling coefficient, and v and w are the displacement field of the solid matrix and fluid, respectively. Introducing scale factors for each of the variables: $v = w_0\hat{v}$, $w = w_0\hat{w}$, $\sigma = P_0\hat{\sigma}$,$P = P_0\hat{P}$, $z = L\hat{z}$, and $t = t_0\hat{t}$, where $t_0 = (2\pi f)^{-1}$, and f is the forcing frequency in s^{-1}. Assigning the scale factors in equation (A5), dropping the $\hat{}$ notation, and considering the magnitude of the densities ρ_f, ρ_b and the coupling coefficient m to be of the same order:

$$\begin{aligned} \frac{w_0\rho_f L(2\pi f)^2}{P_0}\left(\frac{\partial^2 v}{\partial t^2} + \frac{\partial^2 w}{\partial t^2}\right) &= \frac{\partial \sigma}{\partial z} \\ \frac{w_0\rho_f L(2\pi f)^2}{P_0}\left(\frac{\partial^2 v}{\partial t^2} + \frac{\partial^2 w}{\partial t^2}\right) &= \frac{\partial P}{\partial z} + \frac{\mu w_0 L(2\pi f)}{kP_0}\frac{\partial w}{\partial t}. \end{aligned} \tag{A6}$$

Taking $\rho_f = 10^3$ kg m^{-3}, $L = 1$ m, $P_0 = 100$ Pa, and $w_0 = 10^{-7}$ m following the value used in *Bachrach et al.* [2001], it is found that the acceleration terms, lefthand side of equation (A6), are important only for frequencies of the order ≥ 100 Hz. Thus, for smaller frequencies *Bachrach et al.* [2001] formulation is equivalent to *Wang* [2000, equation (6.14)] formulation, which by itself was shown to be similar to our equation (10).

A2. Non-Elastic Formulations

Walder and Nur [1984] study processes of PP generation due to porosity reduction, accounting also for non-elastic deformation [*Walder and Nur*, 1984, equation (5)]:

$$\frac{\partial P}{\partial t} = \frac{k}{\mu\Phi(\beta+\beta_\Phi)}\nabla^2 P - \frac{1}{\Phi(\beta+\beta_\Phi)}\frac{\partial \Phi}{\partial t}_{irrev}. \tag{A7}$$

In this formulation, $\beta_\Phi = (1/\Phi)(\partial\Phi/\partial P)$ is the elastic pore compressibility, and $(\partial\Phi/\partial t)_{irrev}$ is the irreversible porosity evolution. With some algebraic transformation equation (A7) may be rewritten as:

$$\frac{\partial P}{\partial t} = \frac{k}{\mu\Phi\beta}\nabla^2 P - \frac{1}{\Phi\beta}\left(\frac{\partial \Phi}{\partial t}_{rev} + \frac{\partial \Phi}{\partial t}_{irrev}\right) \tag{A8}$$

where the pore compressibility was expanded as $\beta_\Phi = (1/\Phi)(\partial\Phi/\partial t)_{rev}(\partial t/\partial P)$, and $(\partial\Phi/\partial t)_{rev}$ is the reversible component of the porosity change. Equation (A8) resembles our equation (15) under the assumption of space independent permeability. The forcing term of equation (A8) that is divided between reversible and irreversible porosity reduction is expressed as a single term in our equation (15). Therefore the forcing terms are identical up to a factor of $(1-\Phi)$. This factor results from the different definitions of Darcy's velocity: *Walder and Nur* [1984] use $\mathbf{u_f} = -\frac{k}{\mu\Phi}\nabla P$ as if the matrix is stationary, while our formulation assumes that Darcy's velocity is given by equation (3).

This section demonstrated that former formulation of PP generation by porous or granular matrix deformation may be reduced to our equations (10) or (15). That is, the formulations of *Wang* [2000]; *Bachrach et al.* [2001]; *Walder and Nur* [1984] and the formulations of *Snieder and van der Beukel* [2004] and *Samuelson et al.* [2009] that are not discussed here, all describe the temporal evolution of PP as a combination of diffusion term and a forcing term.

Appendix B: Analytical Prediction for a Large System (B.C. of Type 3)

Here we derive an analytical prediction for the temporal and spatial evolution of the PP for the model of fluid-filled uniform granular material packed in hexagonal packing under constant shear velocity that is presented in section 4.1. This solution applies to the case of a large system with $\zeta \gg l_k$, denoted as B.C. of type 3. The prediction is derived by solving equation (10) under the assumption of constant diffusion coefficient, $D_c = k_{min}/\beta\mu\Phi_{min}$, and using the granular velocity and porosity from equation (18). The equation to be solved is:

$$\frac{\partial P}{\partial t} = D_c \frac{\partial^2 P}{\partial z^2} - \frac{1}{\beta} H(z,t), \tag{B1}$$

where $H(z,t)$ expresses the forcing $\nabla \cdot u_{sz}/\Phi$ that is concentrated along $z = 0$ (the shearing row) and is defined as:

$$H(z,t) = \delta(z) V_{sh} \cdot u_H(t), \quad 0 < t < t_0 = d/V_{sh}, \tag{B2}$$

and

$$u_H(t) = \frac{u_{sz}}{\Phi} = \frac{(0.5 - t/t_0)}{\sqrt{1 - (0.5 - t/t_0)^2} - \pi/4}. \tag{B3}$$

$\delta(z)$ is Dirac delta function with units of m^{-1} and it stands for the ∇ operator in equation (10). The solution of equation (B1) for $P(z,t)$ may be expressed using a Green's function

by the integral [*McKenzie and Brune*, 1972]:

$$P(z,t) = -\frac{1}{2\beta\sqrt{D_c\pi}} \int_0^t \int_{-\infty}^{\infty} \exp\left[-\frac{(z-z_i)^2}{4D(t-t_i)}\right] \frac{H(z_i,t_i)}{\sqrt{t-t_i}} dz_i dt_i. \tag{B4}$$

Assigning $H(z_i,t_i)$ from equation (B2), equation (B4) is evaluated as [*McKenzie and Brune*, 1972]:

$$P(z,t) = -\frac{V_{sh}}{2\beta\sqrt{D\pi}} \int_0^t \exp\left[-\frac{z^2}{4D(t-t_i)}\right] \frac{u_H(t_i)}{\sqrt{t-t_i}} dt_i. \tag{B5}$$

To solve equation (B5) we first expand $u_H(t_i)$ as a third order power series of t_i using its third order interpolation polynomial, i.e. $u_H(t_i) = \sum_{j=0}^{j=3} a_j (t_i)^j$. Next $u_H(t_i)$ is rewritten as a third order power series of $(t-t_i)$, $u_H(t_i) = \sum_{j=0}^{j=3} b_j (t-t_i)^j$, where $b_j = b_j(t)$ is found by solving the system of linear equations:

$$\begin{aligned} b_0(t) &= a_0 + a_1 t + a_2 t^2 + a_3 t^3 \qquad \text{(B6)} \\ b_1(t) &= -a_1 - 2a_2 t - 3a_3 t^2 \\ b_2(t) &= a_2 + 3a_3 t \\ b_3(t) &= -a3, \end{aligned}$$

and equation (B5) is rewritten as:

$$P(z,t) = -\frac{V_{sh}}{2\beta\sqrt{D\pi}} \int_0^t \exp\left[-\frac{z^2}{4D(t-t_i)}\right] \frac{\sum_{j=0}^{j=3} b_j (t-t_i)^j}{\sqrt{t-t_i}} dt_i. \tag{B7}$$

Next the following dimensionless variables are defined [*McKenzie and Brune*, 1972]:

$$\begin{aligned} \hat{P} &= \frac{\beta\sqrt{\pi D d/V_{sh}}}{d} P \qquad \text{(B8)} \\ \hat{t}_i &= t_i/t_0 \\ \hat{t} &= t/t_0 \\ \hat{z} &= \frac{1}{\sqrt{2D_c t_0}} z \end{aligned}$$

and equation (B7) may be written in a non-dimensional form:

$$\begin{aligned}
\hat{P}(\hat{z},\hat{t}) &= -\frac{1}{2}\int_0^{\hat{t}} \exp\left[-\frac{\hat{z}^2}{2(\hat{t}-\hat{t}_i)}\right] \frac{\sum_{j=0}^{j=3} b_j(\hat{t})(\hat{t}-\hat{t}_i)^j}{\sqrt{\hat{t}-\hat{t}_i}} d\hat{t}_i \qquad \text{(B9)}\\
&= -\left(b_0(\hat{t})\frac{1}{2}\int_0^{\hat{t}} \exp\left[-\frac{\hat{z}^2}{2(\hat{t}-\hat{t}_i)}\right] \frac{1}{\sqrt{\hat{t}-\hat{t}_i}} d\hat{t}_i\right)\\
&\quad -\left(b_1(\hat{t})\frac{1}{2}\int_0^{\hat{t}} \exp\left[-\frac{\hat{z}^2}{2(\hat{t}-\hat{t}_i)}\right] \frac{(\hat{t}-\hat{t}_i)}{\sqrt{\hat{t}-\hat{t}_i}} d\hat{t}_i\right)\\
&\quad -\left(b_2(\hat{t})\frac{1}{2}\int_0^{\hat{t}} \exp\left[-\frac{\hat{z}^2}{2(\hat{t}-\hat{t}_i)}\right] \frac{(\hat{t}-\hat{t}_i)^2}{\sqrt{\hat{t}-\hat{t}_i}} d\hat{t}_i\right)\\
&\quad -\left(b_3(\hat{t})\frac{1}{2}\int_0^{\hat{t}} \exp\left[-\frac{\hat{z}^2}{2(\hat{t}-\hat{t}_i)}\right] \frac{(\hat{t}-\hat{t}_i)^3}{\sqrt{\hat{t}-\hat{t}_i}} d\hat{t}_i\right)\\
&= -\left[b_0(\hat{t})I_0 + b_1(\hat{t})I_1 + b_2(\hat{t})I_2 + b_3(\hat{t})I_3\right],
\end{aligned}$$

where I_i are the integrals. The solution for I_0 from *McKenzie and Brune* [1972] is:

$$I_0 = \sqrt{\hat{t}}\exp\frac{-\hat{z}^2}{2\hat{t}} - \hat{z}\sqrt{\frac{\pi}{2}}\mathrm{erfc}\left(\frac{\hat{z}}{\sqrt{2\hat{t}}}\right). \qquad \text{(B10)}$$

Integrals $I_1 - I_3$ can be integrated in parts and reduced to I_0 as following:

$$\begin{aligned}
I_1 &= \frac{1}{2}\int_0^{\hat{t}} \exp\left[-\frac{\hat{z}^2}{2(\hat{t}-\hat{t}_i)}\right] \frac{(\hat{t}-\hat{t}_i)}{\sqrt{\hat{t}-\hat{t}_i}} d\hat{t}_i \qquad \text{(B11)}\\
&= -\frac{1}{2}\int_{\hat{t}}^{0} \exp\left[-\frac{\hat{z}^2}{2\tau}\right] \tau^{1/2} d\tau\\
&= -\frac{1}{2}\left[\left(\frac{2}{3}\tau^{3/2}\exp\left[-\frac{\hat{z}^2}{2\tau}\right]\right)|_{\hat{t}}^{0} - \frac{2}{3}\frac{\hat{z}^2}{2}\int_{\hat{t}}^{0} \exp\left[-\frac{\hat{z}^2}{2\tau}\right]\tau^{-1/2} d\tau\right]\\
&= \frac{1}{3}\left[\hat{t}^{3/2}\exp\left[-\frac{\hat{z}^2}{2\hat{t}}\right] - \hat{z}^2 I_0\right]
\end{aligned}$$

Similarly, it can be shown that

$$\begin{aligned}
I_2 &= \frac{1}{5}\left[\hat{t}^{5/2}\exp\left[-\frac{\hat{z}^2}{2\hat{t}}\right] - \hat{z}^2 I_1\right] \qquad \text{(B12)}\\
I_3 &= \frac{1}{7}\left[\hat{t}^{7/2}\exp\left[-\frac{\hat{z}^2}{2\hat{t}}\right] - \hat{z}^2 I_2\right].
\end{aligned}$$

Equations (B6) and (B7) - (B12) give a full solution for $\hat{P}(\hat{z},\hat{t})$. Evaluating $\hat{P}(\hat{z},\hat{t})$ along the shearing row gives:

$$P(0,\hat{t})\frac{\beta\sqrt{\pi Dd/V_{sh}}}{d} = -\frac{1}{105}\sqrt{(\hat{t})}(582.929 - 1885.66\hat{t} + 2667.73\hat{t}^2 - 1524.38\hat{t}^3) \quad \text{(B13)}$$

where the coefficient of the interpolation polynomial for $u_H(\hat{t})$ are $a_0 = 5.5517$, $a_1 = -26.938$, $a_2 = 47.638$ and $a_3 = -31.758$. Figure (6) compares equation (B13) to simulation results conducted with constant diffusion coefficient, D_c, and B.C. of type 3. Figure (B8) compares the spatial pattern of PP at the end of the period ($\hat{t} = 1$) between simulations with B.C. of type 3 and the analytical prediction presented here.

Acknowledgments. We thank Amotz Agnon and Michael Tsesarsky for fruitful discussions. We also wish to thank André Niemeijer, the associate editor and an anonymous reviewer for constructive reviews that helped greatly in improving this manuscript.

References

Aharonov, E., and D. Sparks (2002), Shear profiles and localization in simulations of granular materials, *Phys. Rev. E*, *65*(5), doi:10.1103/PhysRevE.65.051302.

Anghel, D. V., M. Strauss, S. McNamara, E. G. Flekkøy, and K. J. Måløy (2006), Grains and gas flow: Molecular dynamics with hydrodynamic interactions (vol 61, pg 4054, 2000), *Phys. Rev. E*, *74*(2), doi:10.1103/PhysRevE.74.029906.

Bachrach, R., A. Nur, and A. Agnon (2001), Liquefaction and dynamic poroelasticity in soft sediments, *J. Geophys. Res.*, *106*(B7), 13,515–13,526.

Biot, M. A. (1941), General theory for three-dimensional consolidation, *J. Appl. Phys.*, *12*(155).

Biot, M. A. (1956a), Theory of propagation of elastic waves in a fluid-saturated porous solid. I. Low-frequency range, *J. Acoust. Soc. Am.*, *28*, 168–178.

Biot, M. A. (1956b), Theory of propagation of elastic waves in a fluid-saturated porous solid. II. Higher frequency range, *J. Acoust. Soc. Am.*, *28*, 179–191.

Biot, M. A. (1962), Mechanics of deformation and acoustic propagation in porous dissipative media, *J. Appl. Phys.*, *33*(4), 1482–1498.

Blanpied, M. L., D. A. Lockner, and J. D. Byerlee (1992), An earthquake mechanism based on rapid sealing of faults, *Nature*, *358*(6387), 574–576.

Casagrande, A. (1936), Characteristics of cohesionless soils affecting the stability of slopes and earth fills, *Journal of the Boston Society of Civil Engineering*, *23*, 13–32.

Castro, G. (1969), *Liquefaction of sands*, Harvard Soil Mechanics Series 87, Harvard University, Cambridge, Massachusetts.

Cetin, K. O., N. Isik, and B. Unutmaz (2004), Seismically induced landslide at Degirmendere Nose, Izmit bay during Kocaeli (Izmit)-Turkey earthquake, *Soil Dyn. Earthquake Eng.*, *24*(3), 189–197, doi:10.1016/j.soildyn.2003.11.007.

Das, M. B. (1993), *Principles of Soil Mechanics*, PWS-Kent, Boston, Mass.

El Shamy, U., and M. Zeghal (2007), A micro-mechanical investigation of the dynamic response and liquefaction of saturated granular soils, *Soil Dyn. Earthquake Eng.*, *27*(8), 712–729, doi:10.1016/j.soildyn.2006.12.010.

Flekkøy, E. G., A. Malthe-Sørenssen, and B. Jamtveit (2002), Modeling hydrofracture, *J. Geophys. Res.*, *107*(B8), doi:10.1029/2000JB000132.

Forterre, Y., and O. Pouliquen (2008), Flows of dense granular media, *Annu. Rev. Fluid. Mech.*, *40*, doi:10.1146/annurev.fluid.40.111406.102142.

955 Gabet, E. J., and S. M. Mudd (2006), The mobilization of debris flows from shallow
956 landslides, *Geomorphology*, *74*, 207–218, doi:10.1016/j.geomorph.2005.08.013.

957 Garagash, D. I., and J. W. Rudnicki (2003), Shear heating of a fluid-saturated slip-
958 weakening dilatant fault zone 1. limiting regimes, *J. Geophys. Res.*, *108*(B2 2121),
959 doi:10.1029/2001JB001653.

960 Garga, V. K., and H. Zhang (1997), Volume changes in undrained triaxial tests on sands,
961 *Can. Geotech. J.*, *34*, 762–772.

962 Itasca (2005), *PFC3D (Particle Flow Code in 3 Dimensions), Version 3.1.*, Itasca Con-
963 sulting Group, Inc., Minneapolis, Minnesota: Itasca.

964 Iverson, R. M. (2005), Regulation of landslide motion by dilatancy and pore pressure
965 feedback, *J. Geophys. Res.*, *110*(F2), F02015, doi:10.1029/2004JF000268.

966 Iverson, R. M., M. E. Reid, N. R. Iverson, R. G. LaHusen, M. Logan, J. E. Mann, and
967 D. L. Brien (2000), Acute sensitivity of landslide rates to initial soil porosity, *Science*,
968 *290*(5491), 513–516, doi:10.1126/science.290.5491.513.

969 Johnsen, Ø., R. Toussaint, K. L. Måløy, and E. G. Flekkøy (2006), Pattern formation
970 during air injection into granular materials confined in a circular Hele-Shaw cell, *Phys.*
971 *Rev. E*, *74*(1), doi:10.1103/PhysRevE.74.011301.

972 Johnsen, Ø., R. Toussaint, K. J. Måløy, E. G. Flekkøy, and J. Schmittbuhl (2007),
973 Coupled air/granular flow in a linear Hele-Shaw cell, *Phys. Rev. E*, *77*(1), doi:
974 10.1103/PhysRevE.77.011301.

975 Johnsen, Ø., C. Chevalier, A. Lindner, R. Toussaint, E. C. K. J. Måløy, E. G. Flekkøy,
976 and J. Schmittbuhl (2008), Decompaction and fluidization of a saturated and confined
977 granular medium by injection of a viscous liquid or a gas, *Phys. Rev. E*, *78*(5), doi:

10.1103/PhysRevE.78.051302.

Kawakami, F., and A. Asada (1966), Damage to the ground and earth structures by the Niigata earthquake of june 16,1964, *Soil and foundation*, *6*(1), 14–30.

Kherbouche, R., J. F. Shao, F. Skoczylas, and J. P. Henry (1995), On the poroplastic behavior of porous rocks, *Eur. J. Mech. A. Solids*, *14*(4), 577–587.

Kostadinov, M. V., and I. Towhata (2002), Assessment of liquefaction-inducing peak ground velocity and frequency of horizontal ground shaking at onset of phenomenon, *Soil Dyn. Earthquake Eng.*, *22*(4), 309 – 322, doi:10.1016/S0267-7261(02)00018-0.

Kozlov, V. G., A. A. Ivanova, and P. Evesque (1998), Sand behavior in a cavity with incompressible liquid under vertical vibrations, *Europhys. Lett.*, *42*(3), 413–418.

Kramer, S. L. (1996), *Geotechnical earthquake engineering*, Prentice Hall, Inc., Upper Saddle River, New Jersey.

Li, X., X. Chu, and D. Sheng (2007), A saturated discrete particle model and characteristic-based sph method in granular materials, *Int. J. Numer. Methods Eng.*, *72*, 858–882, doi:10.1002/nme.2037.

Manzari, M. T., K. Arulanandan, and R. F. Scott (1994), VELACS project: A summary of achievements, in *Proceedings from the Fifth U.S.-Japan Workshop on Earthquake Resistant Design of Lifeline Facilities and Countermeasures Against Liquefaction*, edited by T. D. O'Rourke and M. Hamada, National Center for Earthquake Engineering Research, State University of New York Buffalo, technical Report NCEER-940-0026.

Marone, C., C. B. Raleigh, and C. H. Scholz (1990), Frictional behavior and constitutive modeling of simulated fault gouge, *J. Geophys. Res.*, *95*, 7007–7025.

McKenzie, D., and J. N. Brune (1972), Melting on fault planes during large earthquakes, *Geophys. J. R. Astr. Soc.*, *29*, 65–78.

McNamara, S., E. G. Flekkøy, and K. J. Måløy (2000), Grains and gas flow: Molecular dynamics with hydrodynamic interactions, *Phys. Rev. E*, *61*(4), 4054 – 4059.

Miller, S. A., and A. Nur (2000), Permeability as a toggle switch in fluid-controlled crustal processes, *Earth Planet. Sci. Lett.*, *183*, 133–146.

Moore, P. L., and N. R. Iverson (2002), Slow episodic shear of granular materials regulated by dilatant strengthening, *Geology*, *30*(9), 843–846.

Mourgues, R., and P. Cobbold (2003), Some tectonic consequences of fluid overpressures and seepage forces as demonstrated by sandbox modelling, *Tectonophysics*, *376*(1-2), 75–97, doi:10.1016/S0040-1951(03)00348-2.

Okada, Y., and H. Ochiai (2007), Coupling pore-water pressure with distinct element method and steady state strengths in numerical triaxial tests under undrained conditions, *Landslides*, *4*, 357–369, doi:10.1007/s10346-007-0092-1.

Popescu, R., and J. H. Prevost (1995), Comparison between VELACS numerical class-A predictions and centrifuge experimental soil test-results, *Soil Dyn. Earthquake Eng.*, *14*(2), 79–92.

Rozhko, A. Y., Y. Y. Podladchikov, and F. Renard (2007), Failure patterns caused by localized rise in pore-fluid overpressure and effective strength of rocks, *Geophys. Res. Lett.*, *34*(22), doi:10.1029/2007GL031696.

Samuelson, J., D. Elsworth, and C. Marone (2009), Shear induced dilatancy of fluid saturated faults: experiment and theory, *J. Geophys. Res.*, doi:10.1029/2008JB006273, in press.

Sawicki, A., and J. Mierczynski (2006), Developments in modeling liquefaction of granular soils, caused by cyclic loads, *Appl. Mech. Rev.*, *59*, 91–106, doi:10.1115/1.2130362.

Scawthorn, C., and P. I. Yanev (1995), Preliminary report 17 January 1995, Hyogo-ken Nambu, Japanese earthquake, *Eng. Struct.*, *17*(3), 146–157.

Scholz, C. H. (1990), *The mechanics of earthquakes and faulting*, Cambridge University Press.

Segall, P., and J. R. Rice (1995), Dilatancy, compaction, and slip instability of fluid-infiltrated fault, *J. Geophys. Res.*, *100*(B11), 22,155–22,171.

Sidle, R. C., and H. Ochiai (2006), *Landslides processes, Prediction, and Land Use*, American Geophysical Union, Washington, DC.

Skempton, A. W. (1960), Terzaghi's discovery of effective stress, in *From Theory to Practice in Soil Mechanics*, edited by L. Bjerrum, A. Casagrande, R. B. Peck, and A. W. Skempton, pp. 42–53, John Wiley, New York.

Sleep, N. H., and M. L. Blanpied (1992), Creep, compaction and the weak rheology of major faults, *Nature*, *359*(6397), 687–692.

Snieder, A., and A. van der Beukel (2004), The liquefaction cycle and the role of drainage in liquefaction, *Granular Matter*, *6*, doi:10.1007/s100035-0030151-9.

Soga, K. (1998), Soil liquefaction effects observed in the Kobe earthquake of 1995, *Proceedings Of The Institution Of Civil Engineers-Geotechnical Engineering*, *131*(1), 34–51.

Terzaghi, K. (1943), *Theoretical Soil Mechanics*, John Wiley, New York.

Vinningland, J. L., Ø. Johnsen, E. G. Flekkøy, R. Toussaint, and K. J. Måløy (2007a), Granular Rayleigh-Taylor instability: Experiments and simulations, *Phys. Rev. Lett.*, *99*(4), doi:10.1103/PhysRevLett.99.048001.

Vinningland, J. L., Ø. Johnsen, E. G. Flekkøy, R. Toussaint, and K. J. Måløy (2007b), Experiments and simulations of a gravitational granular flow instability, *Phys. Rev. E*, *76*(5), doi:10.1103/PhysRevE.76.051306.

Voight, B., and C. Faust (1982), Frictional heat and strength loss in some rapid landslides, *Géotechnique*, *32*(1), 43–54.

Walder, J., and A. Nur (1984), Porosity reduction and crustal pore pressure development, *J. Geophys. Res.*, *89*(B13), 11,539–11,548.

Wang, H. F. (2000), *Theory of Linear Poroelasticity with Applications to Geomechanics and Hydrogeology*, Princeton University Press, Princeton, NJ.

Yamashita, T. (1999), ore creation due to fault slip in a fluid-permeated fault zone and its effect on seismicity: Generation mechanism of earthquake swarm, *Pure Appl. Geophys.*, *155*, 625–647.

Youd, T. L. (1972), Compaction of sands by repeated shear straining, *Journal of Soil Mechanics and Foundations Design*, *98*, 709–725.

Zienkiewicz, O. C., A. H. C. Chan, M. Pastor, B. A. Schrefler, and T. Shiomi (1999), *Computational Geomechanics with Special Reference to Earthquake Engineering*, J. Wiley, Chichester.

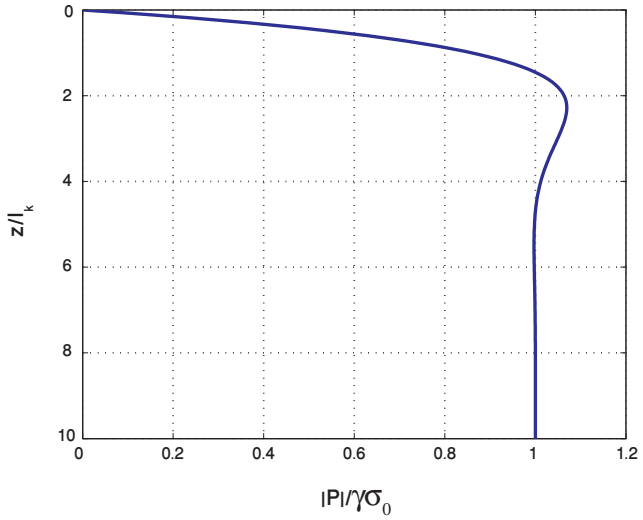

Figure 1. Half space solution of system of equations (16) and (17), describing the spatial evolution of PP in a poroelastic material under periodic stress loading and drained top. Maximum magnitude of PP, $|P|$, is plotted as a function of normalized depth. $|P|$ is bounded by $1.07\gamma\sigma_0$, where $\gamma \leq 1$ is the loading efficiency and σ_0 is the amplitude of the pressure wave forcing. The relation between $|P|$ and σ_0 indicates that a poroelastic mechanism for liquefaction (see text) is limited to the very top of the soil column. Adopted from *Wang* [2000, Figure 6.11].

Table 1. Model parameters for section 4.1

Symbol	Parameter	Value
β	Water compressibility	4.5×10^{-10} Pa^{-1}
μ	Water viscosity	10^{-3} Pa s
d	Grain diameter	5×10^{-4} m
h	Granular layer thickness for B.C. of types 1, 2	0.01 m
	Granular layer thickness for B.C. of type 3	4 m
V_{sh}	Shearing velocity	0.1 m/s
Φ_{min}	Porosity of hexagonal packing	0.093
k	Permeability (Carman-Kozeny)	$d^2\Phi^3/180(1-\Phi)^2$ m^2
D	Diffusion coefficient	$D_c = k_{min}/\beta\mu\Phi_{min} = 32.45$ m^2/s*
l_k	PP skin depth	$\sqrt{2D_c t_0} = 0.57$ m †

* Value corresponds to the constant diffusion coefficient used in the analysis of a large system (B.C. of type 3)

† Value corresponds to diffusion length scale calculated for the constant diffusion coefficient of a large system analysis.

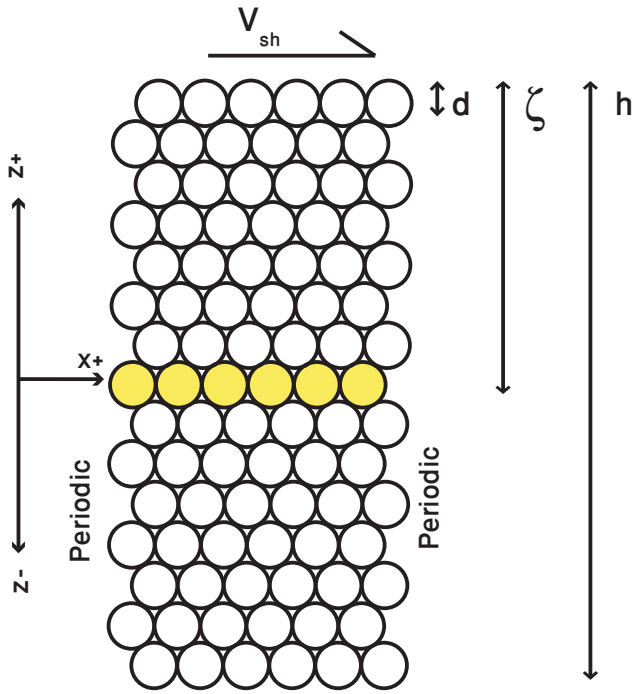

Figure 2. Model geometry for section 4.1. An hexagonal packing of fluid-filled granular material is being subjected to a constant shear velocity, V_{sh}. Shear displacement is accommodated along a single row marked by the yellow grains. The boundaries along the x direction are periodic and therefore, $\partial \mathbf{u_{sx}}/\partial x = 0$. d is a grain diameter, ζ is the distance to the boundary, and h is system thickness.

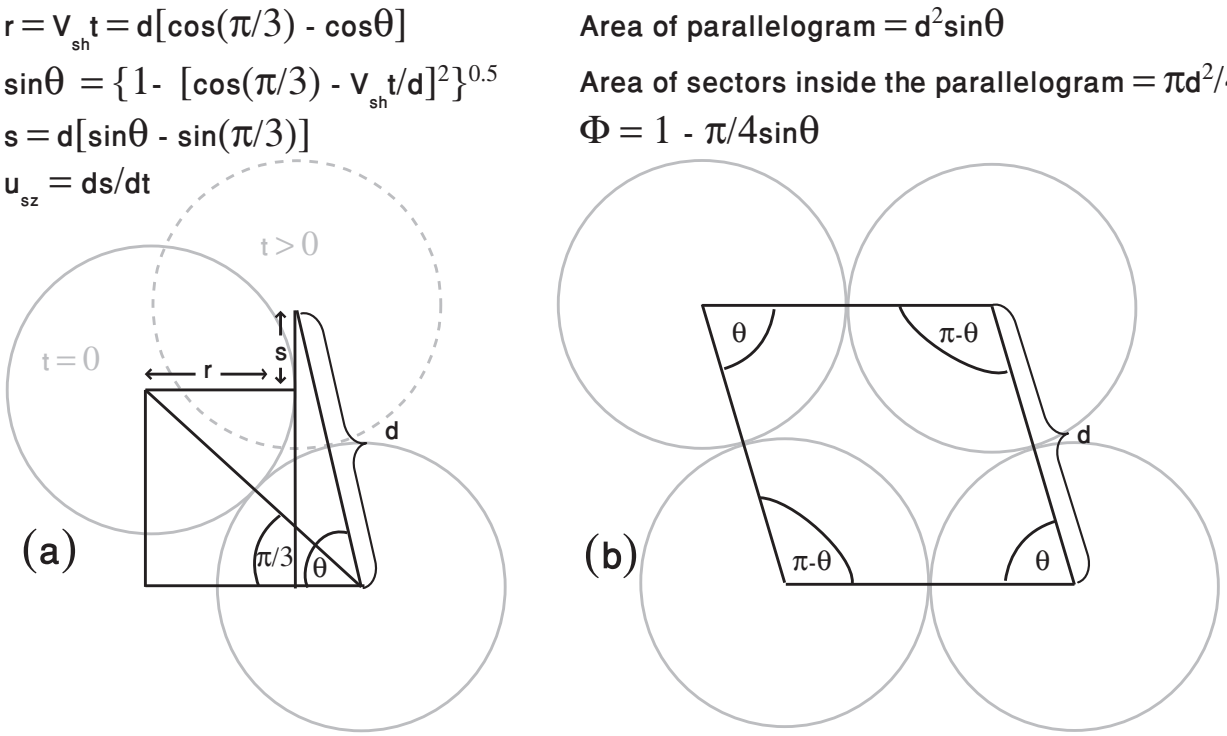

Figure 3. (a) Geometrical relations used for expressing $\mathbf{u_{sz}}$. s is the vertical displacement, θ is the contact angle between grains that depends on V_{sh}, t and d. $\mathbf{u_{sz}}$ is the time derivative of s. (b) Geometrical relations used for expressing the porosity, Φ.

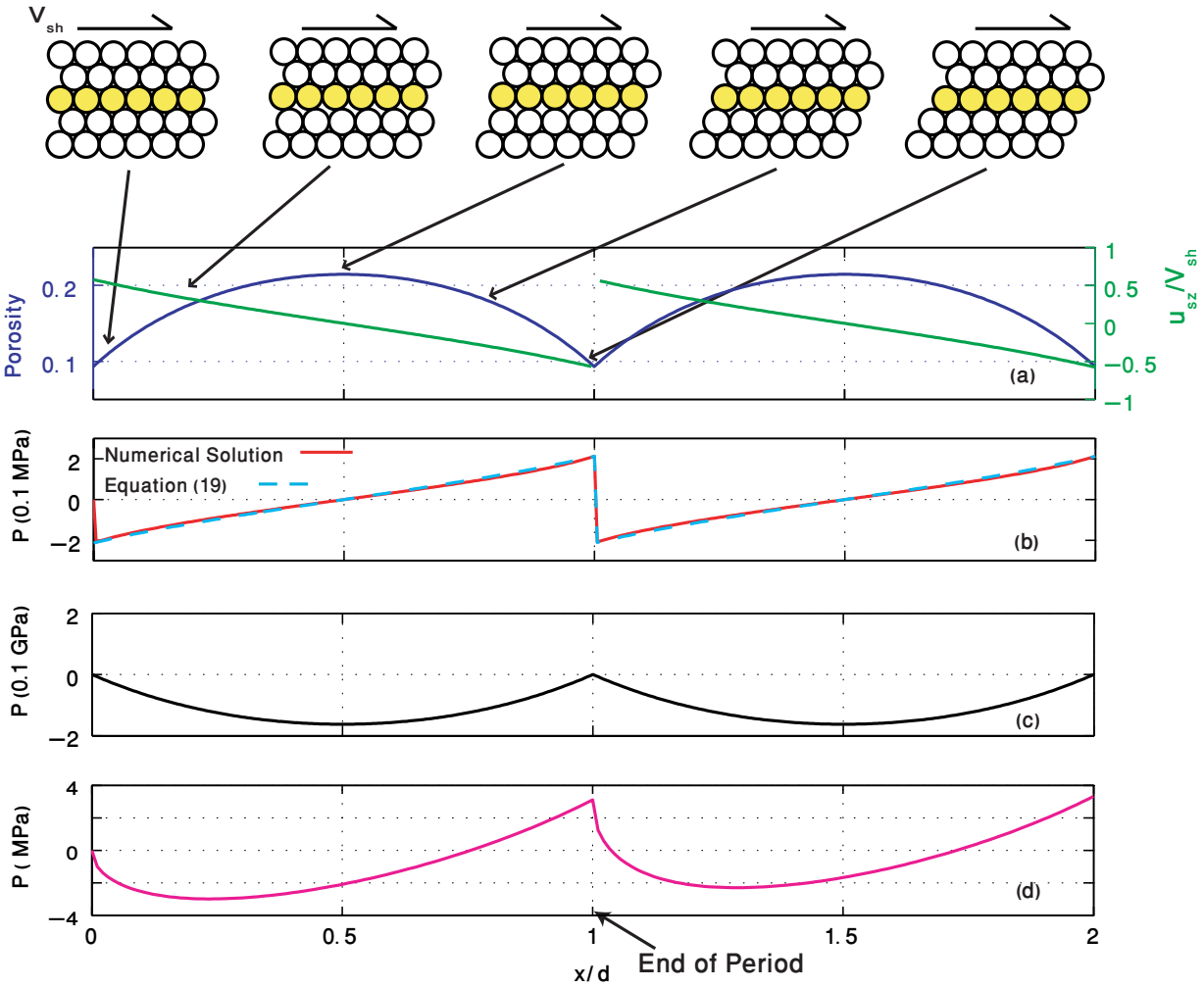

Figure 4. Simulation results of shearing of densely packed fluid-filled granular material at a constant shear velocity, V_{sh}, with parameters from Table 1. Shear is accommodated in a localized manner along a single sliding row, depicted by yellow filled discs. The system first dilates to a cubic packing and then compacts back to a hexagonal packing. Dilation and compaction induce time and space dependent porosity, permeability and granular velocity. (a) Evolution of porosity (blue) and $\mathbf{u_{sz}}/V_{sh}$ (green) along the sliding row as a function of the horizontal displacement, x, scaled by grain diameter, d. (b) PP evolution along the sliding row that accommodates dilation and compaction, when the top boundary is drained, and $\zeta \ll l_k$ (B.C. of type 1). Maximum PP of 0.21 MPa is attained at the end of the period and corresponds to zero effective stress at depth of around 14 m. Red curve is the simulation results and turquoise dashed curve is an analytical prediction following equation (19). (c) PP evolution along the sliding row when the top boundary is undrained with $\zeta \ll l_k$ (B.C. of type 2), showing that PP becomes increasingly negative when the system dilates and then returns to zero upon compaction. (d) PP evolution along the sliding row when $\zeta \gg l_k$ (B.C. of type 3). A combination of the two previous regimes

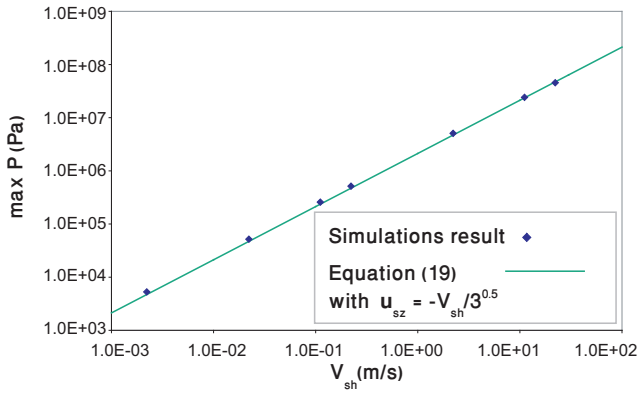

Figure 5. Simulation results with B.C. of type 1 (blue diamonds) for the relation between shear velocity V_{sh} and the maximum value of PP attained at the end of a shearing period. Analytic curve for the same relation (green) is plotted based on equation (19) and the relation $\mathbf{u_{sz}} = -V_{sh}/\sqrt{3}$ that applies to the end if the period (see text), with Table 1 parameters and permeability, k_{min}, induced by hexagonal packing porosity. The slope of the linear relation between P and V_{sh} is a function of fluid viscosity, distance to drainage and inverse of permeability.

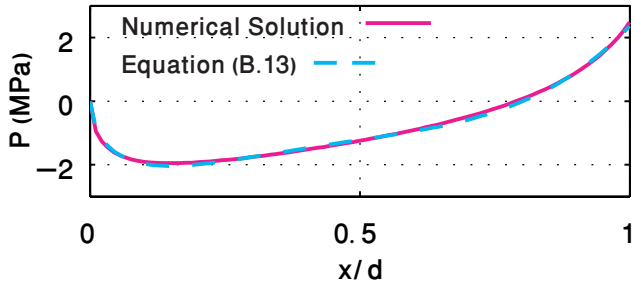

Figure 6. PP along the shearing row for large system (B.C. of type 3), when the diffusion coefficient is assumed constant $D_c = k_{min}/\beta\mu\Phi_{min}$. Purple curve is simulation results and the dashed turquoise curve is the analytical prediction following equation (B13).

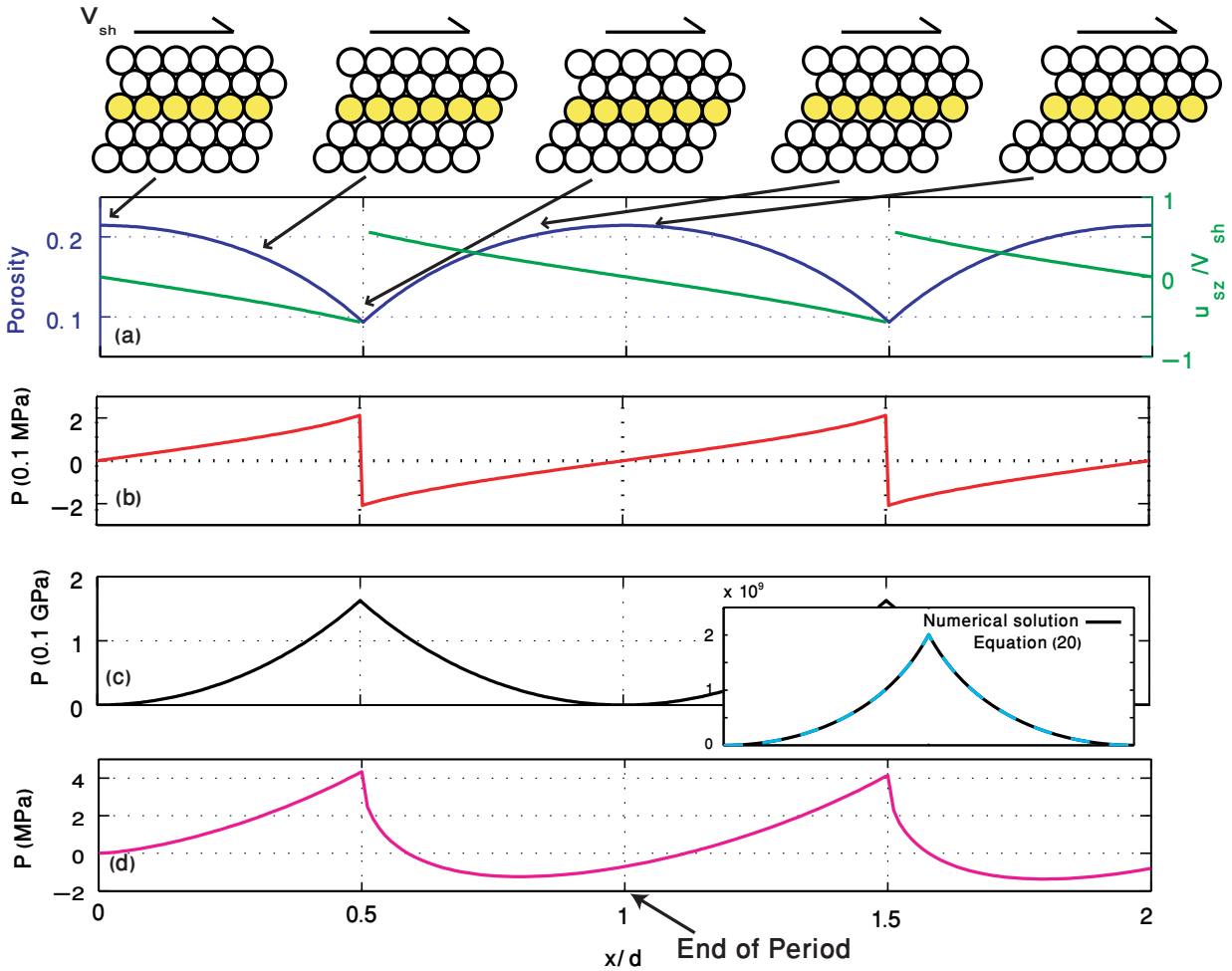

Figure 7. Simulation results of shearing of loosely packed fluid-filled granular material at a constant shear velocity, V_{sh}, with Table 1 parameters. Shear is accommodated in a localized manner along a single sliding row, depicted by yellow filled discs. The system first compacts from a cubic configuration to a hexagonal configuration, and then dilates back to cubic order. (a) Evolution of porosity (blue) and $\mathbf{u_{sz}}$ (green) along the sliding row as a function of the horizontal displacement, x, scaled by grain diameter, d. (b) PP along the sliding row that accommodates compaction and dilation with drained top and $\zeta \ll l_k$ (B.C. of type 1) evolves similarly to shearing of dense packing (Figure (4b)), but with a shift of half period. (c) PP evolution along the sliding row with undrained top and $\zeta \ll l_k$ (B.C. of type 2) showing pore fluid pressurization with maximum of 0.16 GPa, corresponding to zero effective stress at a depth greater than 10 km, in the middle of the period. The inset shows simulation results (black curve) for PP evolution along the sliding row when the permeability is zero throughout the system to oppress PP diffusion, and analytical prediction (turquoise dashed curve) following equation (20) that assumes no diffusion. (d) PP evolution along the sliding row when $\zeta \gg l_k$ (B.C. of type 3), showing a combination of the two previous regimes.

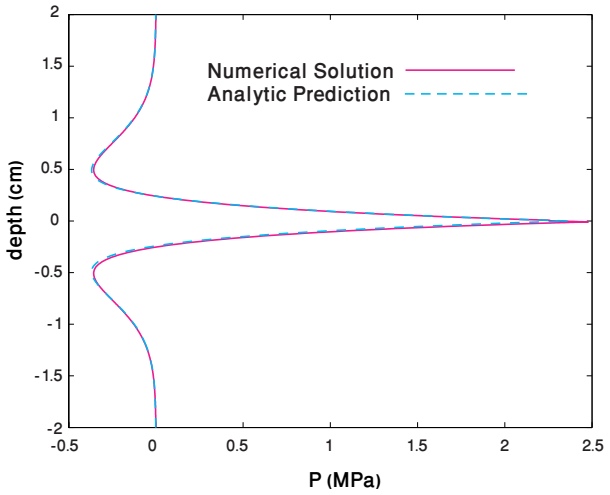

Figure B8. Spatial distribution of PP for a large system (B.C. of type 3) at the end of the period, $\hat{t} = 1$. The shearing row is in the middle of the domain. Purple curve is simulation results and dashed turquoise curve is the analytical prediction for $P(z, d/V_{sh})$ following equations (B6) - (B12).